

Reconciling Consumer and Utility Objectives
in the Residential Solar PV Market

by

Michael R. Arnold

A Thesis Presented in Partial Fulfillment
of the Requirements for the Degree
Master of Science

Approved July 2014 by the
Graduate Supervisory Committee:

Nathan Johnson, Chair
Bradley Rogers
Benjamin Ruddell

ARIZONA STATE UNIVERSITY

August 2014

ABSTRACT

Today's energy market is facing large-scale changes that will affect all market players. Near the top of that list is the rapid deployment of residential solar photovoltaic (PV) systems. Yet that growing trend will be influenced multiple competing interests between various stakeholders, namely the utility, consumers and technology providers. This study provides a series of analyses—utility-side, consumer-side, and combined analyses—to understand and evaluate the effect of increases in residential solar PV market penetration. Three urban regions have been selected as study locations—Chicago, Phoenix, Seattle—with simulated load data and solar insolation data at each locality. Various time-of-use pricing schedules are investigated, and the effect of net metering is evaluated to determine the optimal capacity of solar PV and battery storage in a typical residential home. The net residential load profile is scaled to assess system-wide technical and economic figures of merit for the utility with an emphasis on intraday load profiles, ramp rates and electricity sales with increasing solar PV penetration. The combined analysis evaluates the least-cost solar PV system for the consumer and models the associated system-wide effects on the electric grid. Utility revenue was found to drop by 1.2% for every percent PV penetration increase, net metering on a monthly or annual basis improved the cost-effectiveness of solar PV but not battery storage, the removal of net metering policy and usage of a improved the cost-effectiveness of battery storage and increases in solar PV penetration reduced the system load factor. As expected, Phoenix had the most favorable economic scenario for residential solar PV, primarily due to high solar insolation. The study location—solar insolation and load profile—was also found to affect the time of year at which the largest net negative system load was realized.

TABLE OF CONTENTS

LIST OF TABLES	iii
LIST OF FIGURES	iv
CHAPTER	
1 INTRODUCTION	1
2 REVIEW OF ENERGY SYSTEM MODELING TECHNIQUES AND SOFTWARE	2
Grid Modeling and Asset Planning	2
Modeling Hybrid Power Systems with HOMER	7
Building Energy System Modeling	22
Building Energy Modeling with BEopt	23
3 RECONCILING CONSUMER AND UTILITY OBJECTIVES IN THE RESIDENTIAL SOLAR PV MARKET	25
Abstract	25
Introduction	26
Background	27
Methodological Approach	30
Results and Analysis	39
Discussion and Conclusions	53
REFERENCES	58

LIST OF TABLES

Table	Page
3.1 Household Energy Usage Summary	34
3.2 Grid Rate Structures (\$/kWh)	38
3.3 Residential Market PV Penetration that Produces Negative System Load.....	41
3.4 System Effects of Solar PV Market Penetration.....	42
3.5 Utility Annual Revenue as Percentage of Solar PV Adoption at Max Capacity	43
3.6 Optimal PV Capacities for the Consumer.....	44
3.7 Utility Annual Revenue as Percentage of System-wide Solar PV Capacity	50

LIST OF FIGURES

Figure	Page
3.1 Household Visualization in BEopt.....	32
3.2 Hourly Global Horizontal Solar Radiation at Study Locations	34
3.3 System Net Load Curves at Selected Solar PV Market Penetration Levels	40
3.4 Relative Effects of Solar PV on Electric Grid at 25% Penetration.....	42
3.5 Levelized Cost of Energy for Grid Rate Structures and PV System Sizes	46
3.6 Optimal Power System Configuration Considering Batteries	48
3.7 System Net Load Curves at Optimal Rooftop Capacity for Residences	52

Chapter 1. Introduction

The objective of this thesis was to explore the effects of varying amounts of PV penetration on the net load of a utility for three separate locations across four months of the year. Chapter 2 provides a review of the underlying mathematical formulations used in the modeling software packages HOMER and BEopt. These software packages are implemented in chapter 3 to complete and analysis of the consumer side and utility side implications of high penetration solar PV. Chapter 3 is structured as a draft of a forthcoming journal article.

Modeling approaches and stakeholder engagement efforts that represent and contrast, and perhaps integrate, the perspectives of various parties have proven useful in facilitating energy planning decisions (Loken 2007, Browne et al. 2010). Chapter 3 uses a similar approach to contrast the objectives and desired outcomes of residential ratepayers and an electric utility. A single modeling approach is employed using a common set of input data to generate results that include a collection of possible scenarios in low-, medium- and high-penetration solar PV markets. Rather than focusing on one study site, chapter 3 offers a comparative analysis between three urban regions using simulated load data and solar insolation data at each locality. Various time-of-use pricing schedules are investigated, and the effect of net metering is evaluated to determine the optimal capacity of solar PV and battery storage in a typical residential home. The residential load profile is scaled to assess system-wide technical and economic figures of merit for the utility.

Chapter 2. Review of Energy System Modeling Techniques and Software

Models inform the engineering decision-making process by providing a simulated environment to explore and test design options quickly and at low cost. Energy system models are often used to inform capital acquisition decisions or set equipment operating schedules and limits based upon one or more metrics such as cost, reliability, and environmental impact. Mathematical representations of these metrics are more generally known as objective functions, and with the aid of modeling and simulation, engineers can quickly alter input parameters and evaluate the effect on the objective function to either maximize or minimize a quantity to create an optimal design or decision.

Energy system modeling is a broad field with many specializations and technical focus areas based on the type of energy, scale of the system, and temporal nature of the design decision to be made. Some models focus on the entire electric grid, others on individual buildings, and yet others on smaller scale energy conversion processes such as air conditioners, lighting, and cooking. Many of these models are evaluated in isolation, yet the inputs and outputs of each model do affect systems at different spatial and temporal scales.

2.1 Grid Modeling and Asset Planning

Electric utilities use models for capital expansion planning to inform generation, transmission, and distribution capacity decisions. Modeling the addition or upgrade of electricity generating equipment helps to ensure that the new system will be able to meet the load profile and be cost effective. The optimum capacity expansion plan should take into account capital allocation and equipment selection (Sherali et. al. 1984). The

expansion is an investment in time and money depends on how the equipment is installed in addition to the type of equipment. Commonly known as “soft costs,” the non-hardware costs of permitting, financing, installation labor, and legal work comprise a significant portion of the total cash outlay for capital expansion. Policy issues are also important to consider. New restrictions on emissions and rising fossil fuel prices are pressuring utilities to build more renewable generation. Generation expansion planning models renewables and the cost breakdown to better understand risk (Careri et. al. 2011). There are several software packages for expansion planning. Ventyx’s Strategist is a comprehensive analysis program which examines the costs and benefits of supply resources and their alternatives using real-time market data. In addition, Strategist forecasts resource costs across different market areas using scenario analysis.

The growing number of generation alternatives to coal power plants is increasing the importance of using a robust and comprehensive capital expansion planning software. Coupled with the rising cost of energy from convention sources, except natural gas, evaluating various generation types, technologies, and sizes is vital to making a sound technical and economic decision (Sadorsky 2010). Furthermore, operating assets efficiently has a significant impact on asset performance and life. Production cost modeling follows after capital expansion planning tools to evaluate shorter time horizons for determining how to dispatch existing assets to produce the least-cost power over days or days or weeks into the future. This can be improved by understanding the techno-economic factors associated to energy use and delivery to ensure that new equipment can adequately meet the user’s needs while integrating into the electric grid (Krause et. al. 2010).

Two production cost modeling software tailored specifically to renewables integration include the Hybrid Optimization Model for Electric Renewables (HOMER) authored by the U.S. National Renewable Energy Laboratory (NREL) and RETScreen authored by Natural Resources Canada. HOMER helps to answer questions about the cost effectiveness and supply/demand dynamics of hybrid—nonrenewable and renewable—off-grid and grid power systems. HOMER is a program that takes user inputs, such as costs and components, to simulate and aid in the decision of the optimal mix of nonrenewable generation, renewable generation, and storage in a system. Solar data can be downloaded from the internet from the NREL or NASA database. The software also determine the installation and maintenance costs of a system for the duration of its usable life. RETScreen is an Excel based cost-benefit analysis tool that aids in selecting between different types of renewable energy and energy efficiency technologies. In addition, this program comes with several databases including climate and hydrology. Both HOMER and RETScreen have free downloadable public versions. A similar tool developed by NREL is Renewable Energy Optimization tool (REOpt). REOpt incorporates photovoltaics, solar hot water, wind, biomass, and other renewable technologies into simultaneous models to simulate hourly interactions of multiple system options that go beyond renewables integration and include energy efficiency and various electrical and thermal load options. The System Advisor Model (SAM) is another program developed by NREL and is used to calculate the cost of energy on the client-side or the utility-side of the meter. SAM uses information such as operating costs and system constraints defined by the user to make these cost prediction calculations.

Unit commitment and load dispatch decisions occur hours or days in advance to schedule what generation equipment to have online. Advanced unit commitment and dispatch analyses have been found to save an electric utility millions of dollars each year (Archana et. al. 2012). Deciding where to dispatch individual generating units requires an optimization algorithm, such as genetic algorithms, particle swarm optimization or others that can optimize across non-linear and non-convex spaces. ABB's GridView is one example of such a software that provides energy market simulation and analysis for energy forecasting and management. Analysis methodology combines generation, transmission, loads, fuels and market economics into an integrated framework. Each of these variables is broken into individual optimization, assessment, management and analysis studies. At a smaller scale, the Hybrid Optimization by Genetic Algorithms (HOGA) software provides a simulation and optimization environment for evaluating dispatch options for hybrid renewable energy systems.

Contingency analysis seeks to predict the outcome of a certain set of events, with the goal of planning a response to a failure or unplanned outage (Wong et. al. 2014). This is a useful analysis when paired with reliability analyses of electrical generating equipment. These analyses are often based on probability and are used to determine system robustness and reliability (Kile and Uhlen 2012). As a result, the computations are often data intensive, and require strong software support and computational resources. Siemens' power transmission system planning (PSS/E) uses probabilistic analyses and advanced dynamics modeling to provide design and operation techniques for reliable networks. PSS/E is broken into modules that include dynamic simulation, geomagnetic induced currents, graphical model builder, eigenvalue and modal analysis, optimal power flow and short

circuit calculations. A similar program developed by General Electric's is power systems load flow (PSLF). PSLF allows users to perform transient stability analysis as well as traditional voltage and thermal analyses. General Electric's multi-area production simulation software (MAPS) provides detailed modeling for assessing the value of a portfolio of generation and transmission bottlenecks that constrain economic operation.

Sub-second simulations can be used to describe the transient dynamics the grid system and power electronics. They can be used to determine the effects of various power grid disturbances such as faults, equipment switching, and routine maintenance. Power systems change more frequently than ever before due to market dynamics, random disturbances, increasing grid complexity, and the intermittency of renewables (Fernandopulle and Alden 2005). Simulating transient dynamics helps in determining power system stability. Siemens' PSSNETOMAC facilitates access to and manages information on dynamic power system performance. Some of the methods this tool offers are simulation of transient phenomena, steady-state load flow, frequency analysis, eigenvalue analysis, vibration systems, optimization and others. A similar open-source tool is Open Distribution System Simulator (OpenDSS) offered by the U.S. Department of Energy. It supports distributed resource integration and grid modernization efforts. OpenDSS is a comprehensive electric power system simulation tool designed to meet future needs relating to smart grids, modernization and renewable energy research. These tools can be extended using Spirae's BlueFin software to provide real-time controls analyses that maintain power flow and stability in micro-grids with high-penetration renewables. BlueFin can be installed to operate power systems in real-time using distributed control strategies.

2.2 Modeling Hybrid Power Systems with HOMER

Hybrid power systems incorporate renewable energy sources with non-renewables. Adding renewables to traditional energy generation is done primarily for reducing emissions and reducing delivered energy cost. Hybrid energy systems are popular because they provide many of the benefits of renewable energy while providing dependable operating reserve to manage the intermittency of renewable energy sources (Gupta et. al. 2010). Economic analysis has shown hybrid systems to be more viable than pure renewable or non-renewable energy systems, particularly for off-grid systems (Turkay and Telli 2010). Hybrid systems can be simulated many ways, including genetic algorithms, particle swarm optimization, simulated annealing and others (Erdinc and Uzunoglu 2012). There are also a number of software packages that can simulate hybrid energy systems for viability discussed previously in this text. Hybrid power system modeling and optimization can provide useful information in the early design phase of renewable energy planning.

This thesis uses HOMER for modeling higher renewable penetration scenarios and evaluating the technical and economic impacts during production cost modeling. This is a useful tool during early phases of engineering design. Through three principle tasks (simulation, optimization, and sensitivity analysis), users work with a graphical interface to examine system elements based on technical and economic factors.

- *Simulation* is used to chronologically calculate power output and energy balances hourly for a one-year period. The program seeks to meet electric and thermal demand to supply at each hour with the least cost combination of energy sources. Renewable power generated in each time step is used before nonrenewable power because renewable generators are modeled as sunk costs with no-cost utilization.

The program will establish if the desired system can meet the electric demands while also examining the overall installation and operation cost of the system. A simulation is completed for each combination of equipment and sizes.

- *Optimization* sorts the simulation results by net present cost (NPC)—which is less subject to interpretation than the levelized cost of energy (LCOE). This allows users to quickly review solutions for economic feasibility after HOMER has evaluated solutions on technical feasibility,
- *Sensitivity analysis* is completed by simulating various input values that are outside the engineer’s control (e.g., wind speed, interest rate, equipment costs). HOMER then repeats the optimization step for each combination of sensitivity variables.

Further information regarding HOMER algorithms and functionality can be found in (Lambert 2006). The following sections review the underlying mathematics of the computational model.

2.2.1 Relevant Technical Features

Solar photovoltaic (PV). HOMER simulates PV power output based on a variety of user-inputs such as panel slope and azimuth, a derating factor to account for losses in the installed system, temperature effects and other parameters. The power output of a PV array can be calculated with temperature effects (Eq. 2.1) or without temperature effects (Eq. 2.2).

$$P = Yf\left(\frac{\bar{G}_T}{G_{T,STC}}\right)[1 + \alpha_P(T_c - T_{c,STC})] \quad (2.1)$$

$$P = Yf\left(\frac{\bar{G}_T}{G_{T,STC}}\right) \quad (2.2)$$

P = power output (kW)

Y = rated capacity under standard test conditions (kW)

f = PV derating factor (%)

\bar{G}_T = solar radiation incident on the PV array (kW/m²)

$\bar{G}_{T,STC}$ = incident radiation at standard test conditions (1 kW/m²)

α_p = temperature coefficient of power (%/°C)

T_c = PV cell temperature (°C)

$T_{c,STC}$ = PV cell temperature under standard test conditions (°C)

The effect of temperature on a PV array uses an energy balance equation (Eq. 2.3) that accounts for temperature rises in the panel due to absorption of incident solar (Duffie and Beckman 1991). The energy balance equation can be solved for cell temperature (Eq. 2.4).

$$\tau\alpha G_T = \eta_c G_T + U_L(T_c - T_a) \quad (2.3)$$

$$T_c = T_a + G_T \left(\frac{ta}{U_L} \right) \left(1 - \frac{h_c}{ta} \right) \quad (2.4)$$

τ = solar transmittance (%)

α = solar absorptance (%)

G_T = solar radiation striking the PV array (kW/m²)

η_c = electrical conversion efficiency (%)

U_L = coefficient of heat transfer to the surroundings (kW/m²°C)

T_c = PV cell temperature (°C)

T_a = ambient temperature (°C)

Manufacturers typically report the nominal operating cell temperature (NOCT), defined at an incident radiation of 0.8 kW/m, ambient temperature of 20 °C, and no load. This temperature is used in calculating (Eq. 2.5). HOMER assumes the array is operating at its maximum power point (Eq. 2.6) when calculating the cell temperature (Eq. 2.7).

$$\frac{\tau\alpha}{U_L} = \frac{T_{c,NOCT} - T_{a,NOCT}}{G_{T,NOCT}} \quad (2.5)$$

$$\eta_c = \eta_{mp} \quad (2.6)$$

$$T_c = T_a + (T_{c,NOCT} - T_{a,NOCT}) \left(\frac{G_T}{G_{T,NOCT}} \right) \left(1 - \frac{\eta_{mp}}{\tau\alpha} \right) \quad (2.7)$$

$T_{c,NOCT}$ = nominal operating cell temperature (°C)

$T_{a,NOCT}$ = ambient temperature at which the NOCT is defined (20 °C)

$G_{T,NOCT}$ = solar radiation at which the NOCT is defined (0.8 kW/m²)

η_{mp} = PV efficiency at maximum power point (%)

Efficiency is assumed to vary linearly with temperature according to (Eq. 2.8). PV efficiency decreases with increasing temperature so long as the temperature coefficient of power is negative (Eq. 2.9). Cell efficiency under standard test conditions is defined in (Eq. 2.10).

$$h_{mp} = h_{mp,STC} [1 + a_p (T_c - T_{c,STC})] \quad (2.8)$$

$$T_c = \frac{T_a + (T_{c,NOCT} - T_{a,NOCT}) \left(\frac{G_T}{G_{T,NOCT}} \right) \left[1 - \frac{h_{mp,STC} (1 - a_p T_{c,STC})}{ta} \right]}{1 + (T_{c,NOCT} - T_{a,NOCT}) \left(\frac{G_T}{G_{T,NOCT}} \right) \left(\frac{a_p h_{mp,STC}}{ta} \right)} \quad (2.9)$$

$$\eta_{mp,STC} = \frac{Y}{AG_{T,STC}} \quad (2.10)$$

$\eta_{mp,STC}$ = maximum power point efficiency under standard test conditions (%)

α_p = temperature coefficient of power (%/°C)

$T_{c,STC}$ = cell temperature under standard test conditions (25°C)

A = surface area of PV module (m²)

$G_{T,STC}$ = radiation under standard test conditions (1 kW/m²)

Lead acid battery. HOMER uses the Kinetic Battery Model (KiBaM) to determine battery energy and charge/discharge limits in each time step for a lead acid battery. KiBaM simulates battery electrochemical kinetics by separating the battery into two internal forms of storage—available energy and bound energy (Eq. 2.11)—as a characterization of lead acid battery discharge curves that indicate the total cycle discharged energy decreases with increasing discharge rate (Manwell 1993). HOMER first calculates the maximum charge power (Eq. 2.12) and maximum discharge power (Eq. 2.13) allowed in the time step to serve as a bound on the actual charge power or discharge power determined during economic dispatch. The actual power is then used to determine the total remaining battery energy—sum of available energy (Eq. 2.14) and bound energy (Eq. 2.15)—at the end of each time step. Battery charge and discharge efficiencies are equal to the square root of the battery round trip efficiency.

$$E^t = E_{av} + E_{bnd} \quad (2.11)$$

$$P_{cmax}^t = \frac{kE_{av}^t e^{-k\Delta t} + E^t kc(1 - e^{-k\Delta t})}{1 - e^{-k\Delta t} + c(k\Delta t - 1 + e^{-k\Delta t})} \quad (2.12)$$

$$P_{dmax}^t = \frac{-kE_{max} + kE_{av}^t e^{-k\Delta t} + E^t kc(1 - e^{-k\Delta t})}{1 - e^{-k\Delta t} + c(k\Delta t - 1 + e^{-k\Delta t})} \quad (2.13)$$

$$E_{av}^{t+\Delta t} = E_{av}^t e^{-k\Delta t} + \frac{(E^t kc - P^t)(1 - e^{-k\Delta t})}{k} + \frac{P^t c(k\Delta t - 1 + e^{-k\Delta t})}{k} \quad (2.14)$$

$$E_{bnd}^{t+\Delta t} = E_{bnd}^t e^{-k\Delta t} + E^t (1 - c)(1 - e^{-k\Delta t}) + \frac{P^t (1 - c)(k\Delta t - 1 + e^{-k\Delta t})}{k} \quad (2.15)$$

E^t = total energy (kWh)

E_{av} = available energy (kWh)

E_{bnd} = bound energy (kWh)

P_{cmax}^t = maximum charging power (kW)

k = battery rate constant (hr^{-1})

Δt = change in time (hr)

c = battery capacity (-)

P_{dmax} = maximum discharging power (kW)

E_{max} = maximum battery energy (kWh)

P^t = (kW)

The cost of obtaining energy from the battery is the summation of the cost of energy in the battery and the battery wear cost (Eq. 2.16). Battery wear cost accounts for the cost of degradation and replacement of a battery due to cycling (Eq. 2.17). The battery is replaced when cycling through the total lifetime throughput (Eq. 2.18).

$$C_{e,o} = C_{bw} + C_{e,i} \quad (2.16)$$

$$C_{bw} = \frac{C_{rep,batt}}{N_{batt} Q_{lifetime} \sqrt{\eta_{rt}}} \quad (2.17)$$

$$Q_{lifetime} = fd \left(\frac{q_{max} V_{nom}}{1000W / kW} \right) \quad (2.18)$$

$C_{rep,batt}$ = battery replacement cost (\$)

N_{batt} = number of batteries in bank (-)

η_{rt} = battery roundtrip efficiency (%)

$C_{e,i}$ = cost of energy put into battery (\$)

f = number of cycles to failure (-)

d = depth of discharge (%)

q_{max} = maximum battery capacity (Ah)

V_{nom} = nominal battery voltage (V)

Converter. A system containing alternating current (A/C) and direct current (D/C) uses a converter to translate AC-to-DC and/or DC-to-AC. The converter in HOMER can be uni-directional or bi-directional with a constant efficiency specified in either direction. In reality, converters are much less efficient at low loads.

2.2.2 Relevant Economic and Policy Features

Grid rate structures. HOMER allows a user to input a grid rate structure using the purchased power price, sellback price and demand rate for any block of time in hours. Multiple rates can be entered depending on the monthly of year, weekday or weekend and time of day to reflect peak and shoulder rates. Monthly and net metering are additional

options to take into account extra energy produced that is sold back to the grid at the end of the net metering period. Total annual energy charges are calculated using (Eq. 2.19) for net metering or (Eq. 2.20) without net metering. Annual grid demand charges are calculated using (Eq. 2.21).

$$C_{grid,energy} = \dot{a}_i^{rates} \dot{a}_j^{12} E_{gridpurchases,i,j} C_{power,i} - \dot{a}_i^{rates} \dot{a}_j^{12} E_{gridsales,i,j} C_{sellback,i} \quad (2.19)$$

$$C_{grid,energy} = \sum_i^{rates} \left\{ \begin{array}{ll} E_{netgridpurchases,i} C_{power,i} & \text{if } E_{netgridpurchases} \geq 0 \\ E_{netgridpurchases,i} C_{sellback,i} & \text{if } E_{netgridpurchases} < 0 \end{array} \right\} \quad (2.20)$$

$$C_{grid,demand} = \dot{a}_i^{rates} \dot{a}_j^{12} P_{grid,peak,i,j} C_{demand,i} \quad (2.21)$$

$E_{gridpurchases,i,j}$ = energy purchased from the grid in month j at the rate i (kWh)

$C_{power,i}$ = grid power price for rate i (\$/kWh)

$E_{gridsales,i,j}$ = energy sold to the grid in month j at the rate i (kWh)

$C_{sellback,i}$ = sellback rate for rate i (\$/kWh)

$E_{netgridpurchases,i}$ = annual net grid purchases at the rate i (kWh)

$P_{grid,peak,i,j}$ = peak hourly grid demand in month j at the rate i (kWh)

$C_{demand,i}$ = grid demand rate for rate i (\$/kW/month)

Component pricing. Users can input three cost parameters for a component—initial capital cost, replacement cost, and operating and maintenance cost—that is based on a single unit or the unit’s capacity. These costs are scaled for larger systems (e.g., twice the cost if you install a two wind turbines). HOMER also allows you to input further cost information for multiple units or larger capacity systems to model economies of scale. No

default cost data is provided because costs are highly variable based on time, location and currency.

Cost of energy. HOMER calculates the levelized cost of energy (LCOE) using (Eq. 2.22). Although an important quantity for comparison, HOMER sorts simulation results based on the net present cost (NPC) because the LCOE can be calculated in a variety of ways by different researchers.

$$LCOE = \frac{C_{ann,tot} - c_{boiler} E_{thermal}}{E_{prim,AC} + E_{prim,DC} + E_{def} + E_{grid,sales}} \quad (2.22)$$

$C_{ann,tot}$ = total annualized cost of the system (\$/yr)

c_{boiler} = boiler marginal cost (\$/kWh)

$E_{thermal}$ = total thermal load served (kWh/yr)

$E_{prim,AC}$ = AC primary load served (kWh/yr)

$E_{prim,DC}$ = DC primary load served (kWh/yr)

E_{def} = deferrable load served (kWh/yr)

$E_{grid,sales}$ = total grid sales (kWh/yr)

Net present cost. The user inputs an annual real interest rate to convert between annual and up-front costs (Eq. 2.23). HOMER assumes that the rate of inflation is the same for all costs. This is used in calculating the total net present cost (Eq. 2.24), a quantity which describes the total up-front cost of all costs incurred over the project lifetime. Annualized capital cost (Eq. 2.25) helps to determine the annual cost of capital investment by dividing the total cost over the project lifetime. Another important metric is the

annualized replacement cost (Eq. 2.26), or what it would cost to replace a component through the project lifetime, less the salvage value (Eq. 2.27).

$$i' = \frac{i' - f}{1 + f} \quad (2.23)$$

$$C_{NPC} = \frac{C_{ann,tot}}{CRF(i, R_{proj})} \quad (2.24)$$

$$C_{acap} = C_{cap} CRF(i, R_{proj}) \quad (2.25)$$

$$C_{arep} = C_{rep} f_{rep} SFF(i, R_{comp}) - S \times SFF(i, R_{proj}) \quad (2.26)$$

$$f_{rep} = \left\{ \begin{array}{l} CRF(i, R_{proj}) / CRF(i, R_{rep}), R_{rep} > 0 \\ 0, R_{rep} = 0 \end{array} \right\} \quad (2.27)$$

$$CRF(i, N) = \frac{i(1+i)^N}{(1+i)^N - 1} \quad (2.28)$$

$$R_{rep} = R_{comp} INT\left(\frac{R_{proj}}{R_{comp}}\right) \quad (2.29)$$

$$S = C_{rep} \frac{R_{rem}}{R_{comp}} \quad (2.30)$$

$$R_{rem} = R_{comp} - (R_{proj} - R_{rep}) \quad (2.31)$$

i = real interest rate (%)

i' = nominal interest rate (%)

f = annual inflation rate (%)

$C_{ann,tot}$ = total annualized cost (\$/yr)

C_{cap} = initial capital cost (\$)

C_{rep} = replacement cost of the component (\$)

CRF = capital recovery factor (-)

i = interest rate (%)

N = number of years (-)

R_{proj} = project lifetime (yr)

R_{comp} = lifetime of the component (yr)

R_{rep} = replacement cost duration (yr)

R_{rem} = remaining life of the component at the end of the project lifetime (y)

INT = integer function (-)

SFF = sinking fund factor (-)

2.2.3 *Relevant environmental features*

Solar insolation and incident solar. HOMER can download monthly solar insolation averages from the NREL or NASA database for the typical meteorological year (TMY) using latitude and longitude data input by the user. TMY data represents a typical year of solar insolation based upon historical averages. HOMER uses the monthly solar insolation data to generate synthetic daily solar insolation data, and then takes the synthetic daily solar insolation data to synthetic hourly solar insolation data. These high-resolution synthetic data are generated using algorithms that based upon low-resolution data—monthly data—on clearness index (Graham 1990). Clearness index is a dimensionless number that ranges from zero to one and indicates the fraction of extraterrestrial solar radiation that strikes the earth's surface. The user may also input their own clearness index or solar insolation data on an hourly basis.

Incident radiation on a photovoltaic (PV) array is determined based on the slope and azimuth of the array and a series of equations that describes the sun's daily trajectory as given in (Duffie and Beckman 1991). This trajectory is described by the solar declination (Eq. 2.32)—the latitude where the sun's rays are perpendicular to the earth at noon—and hour angle (Eq. 2.33)—description of solar time based on hour in day. The hour angle is calculated based on the solar time as given in (Eq. 2.34), with the solar time being calculated from the time zone, civil time, longitude and an eccentricity effect as calculated by (Eq. 2.35) and (Eq. 2.36) due to the non-circular movement of the earth around the sun.

$$\delta = 23.45^\circ \sin\left(360^\circ \frac{284+n}{365}\right) \quad (2.32)$$

$$\omega = (t_s - 12hr) \times 15^\circ/hr \quad (2.33)$$

$$t_s = t_c + \frac{\lambda}{15^\circ/hr} - Z_c + E \quad (2.34)$$

$$E = 3.82(0.000075 + 0.001868 \cos B - 0.032077 \sin B - 0.014615 \cos 2B - 0.04089 \sin 2B) \quad (2.35)$$

$$B = 360^\circ \frac{(n-1)}{365} \quad (2.36)$$

n = day of the year (1-365)

λ = longitude ($^\circ$)

t_s = solar time (hr)

t_c = civil (local) time (hr)

Z_c = time zone in hours east of GMT (hr)

E = eccentricity effect (hr)

The zenith angle (Eq. 2.37) is used in several calculations for calculating solar radiation hitting the earth's surface a titled surface (e.g., PV array).

$$\cos \theta_z = \cos \phi \cos \delta \cos \omega \sin \phi \sin \delta \quad (2.37)$$

ϕ = latitude ($^\circ$)

δ = solar declination ($^\circ$)

ω = hour angle ($^\circ$)

θ_z = zenith angle ($^\circ$)

Extraterrestrial normal radiation (Eq. 2.38) is the amount of solar radiation striking the earth's upper atmosphere, whereas extraterrestrial horizontal radiation (Eq. 2.39) is the amount of solar radiation striking a horizontal surface at the top of the atmosphere (Sen 70). HOMER averages the extraterrestrial horizontal radiation over one time step (Eq. 2.40) for use in hourly calculations. Clearness index (Eq. 2.41) is defined as a ratio of the average global horizontal radiation and the average extraterrestrial horizontal radiation. The calculated extraterrestrial horizontal radiation and the synthetic clearness index from Graham's algorithms is used to calculate the global horizontal radiation.

$$G_{on} = G_{sc} \left(1 + 0.033 \cos \frac{360n}{365}\right) \quad (2.38)$$

$$G_o = G_{on} \cos \theta_z \quad (2.39)$$

$$\bar{G}_o = \frac{12}{\pi} G_{on} \left[\cos \phi \cos \delta (\sin \omega_2 - \sin \omega_1) + \frac{\pi(\omega_2 - \omega_1)}{180^\circ} \sin \phi \sin \delta \right] \quad (2.40)$$

$$k_T = \frac{\bar{G}}{\bar{G}_o} \quad (2.41)$$

G_{on} = extraterrestrial normal radiation (kW/m²)

G_{sc} = solar constant (1.367 kW/m²)

n = day of the year (-)

G_o = extraterrestrial horizontal radiation (kW/m²)

\bar{G} = average global horizontal radiation (kW/m²)

\bar{G}_o = average extraterrestrial horizontal radiation (kW/m²)

ω_1 = hour angle at the beginning of the time step (°)

ω_2 = hour angle at the end of the time step (°)

k_T = clearness index (-)

The total global horizontal insolation (or global horizontal radiation) is a summation of beam radiation and diffuse radiation from the sun (Eq. 2.42); diffuse radiation is bent by the atmosphere while beam radiation is not. HOMER splits the total horizontal radiation into the beam and diffuse components using the diffuse fraction (Eq. 2.43) as a function of the clearness index (Erbs et. al. 1981).

$$\bar{G} = \bar{G}_b + \bar{G}_d \quad (2.42)$$

$$\frac{\bar{G}_d}{\bar{G}} \left\{ \begin{array}{ll} 1.0 - 0.09k_T & \text{for } k_T \leq 0.22 \\ 0.9511 - 0.1604k_T + 4.388k_T^2 - 16.638k_T^3 + 12.336k_T^4 & \text{for } 0.22 < k_T \leq 0.80 \\ 0.165 & \text{for } k_T > 0.80 \end{array} \right\} \quad (2.43)$$

\bar{G}_b = beam radiation (kW/m²)

\bar{G}_d = diffuse radiation (kW/m²)

The beam and diffuse radiation components on the horizontal surface can then be used to calculate the total incident solar on a tilted surface (e.g., PV array) using another series calculations (Eq. 2.44–2.48). The amount of circumsolar diffuse radiation is

determined by the anisotropy index (Eq. 2.46). Horizon brightening (Eq. 2.47) describes how the sun is brightest when at the horizon. The slope and azimuth of the panel are used in the final calculation of total incident solar on the tilted surface (Eq. 2.48).

$$\begin{aligned} \cos q = & \sin d \sin f \cos b - \sin d \cos f \sin b \cos g + \cos d \cos f \cos b \cos w \\ & + \cos d \sin f \sin b \cos g \cos w + \cos d \sin b \sin g \sin w \end{aligned} \quad (2.44)$$

$$R_b = \frac{\cos \theta}{\cos \theta_z} \quad (2.45)$$

$$A_i = \frac{\bar{G}_b}{\bar{G}_o} \quad (2.46)$$

$$f = \sqrt{\frac{\bar{G}_b}{\bar{G}}} \quad (2.47)$$

$$\bar{G}_T = (\bar{G}_b + \bar{G}_d A_i) R_b + \bar{G}_d (1 - A_i) \left(\frac{1 + \cos \beta}{2} \right) \left[1 + f \sin^3 \left(\frac{\beta}{2} \right) \right] + \bar{G} \rho_g \left(\frac{1 - \cos \beta}{2} \right) \quad (2.48)$$

θ = angle of incidence ($^\circ$)

β = slope of the surface ($^\circ$)

γ = azimuth of the surface ($^\circ$)

ρ_g = ground reflectance (%)

2.3 Building Energy System Modeling

Building energy system modeling focuses on determining energy consumption and life cycle costs as a function of building design, occupancy, thermal conditioning, water and energy use. Whole-systems building design uses these and other inputs to provide the user with a great amount of flexibility for modeling different scenarios. Yet in noting that the quality of results depends on the quality of inputs, the input conditions must be researched and well-defined.

Optimizing a building energy system goes beyond the selection of power generation, storage or consumption devices in the building. For example, the placement of windows and building orientation can effect power consumption—e.g., large southward facing windows can reduce the use of heating systems because more sunlight enters and warms the building. Some software packages allow users to evaluate and contrast the effects of building design decisions and equipment decisions on technical, environmental and economic metrics. Examples include free-access simulation tools such as EnergyPlus, eQUEST and BEopt.

EnergyPlus is a text-based building energy simulation program designed to model power, thermal and water usage. EnergyPlus is supported by add-ons, such as OpenStudio, which provide various graphical user interfaces (GUIs) or additional computational support. Another command line simulation engine is DOE-2. The makers of DOE-2 also supply the Quick Energy Simulation Tool (eQUEST), which provides a GUI to access the DOE-2 simulation engine. Yet another tool is Building Energy Optimization (BEopt), which is commonly used to evaluate options for whole-building energy savings in existing and new construction projects. BEopt was created to assist in pursuit of net zero energy buildings. It provides detailed analysis based on building size, occupancy, location and build structure. BEopt provides a GUI and requires a simulation engine such as EnergyPlus to run. Integrating various modeling programs that serve different functions facilitate whole-building energy savings. Such a solution has been described as the interoperability workbench (Augenbroe et. al. 2004). A workbench integrates different file formats for the purpose of combining the design and analysis phase. Integrating various computational models for whole-systems building design and analysis can be useful in assessing all

factors that affect engineering designs, but some researchers suggest caution because model data translation errors and model misuse can lead to spurious conclusions (Nall and Crawley 2011).

Building emulators couple computer-based simulations with actual building hardware to analyze control system performance (Dexter and Havest 1993). Control system efficacy is an important marker of energy consumption. A control system must be able to operate efficiently and effectively to properly modulate energy consumption—e.g., use controllable loads such as a pool pump when excess renewable generation is available or when the grid power price is low. However, some researchers contest that today's buildings emulators (and their users) create a poor representation of reality by relying on a large number of assumptions to reduce unknowns (Bushby et. al. 2010).

2.4 Building Energy Modeling with BEopt

This thesis uses BEopt for modeling hourly home energy use and solar insolation across an entire year. BEopt was created to help engineers and policy makers reach the goal of zero net energy (ZNE) buildings (Christensen 2010). ZNE buildings produce as much electricity as they consume. BEopt uses a basic building geometry—and a series of simulation options—to calculate hourly and total energy usage over a year. Design options include the type of lighting, location and size of windows, HVAC designs, building materials and many more features. In analysis mode, BEopt analyzes design conditions to provide hourly energy use, temperature, humidity, ambient conditions and cooling loads. Output is provided in easy to read tables and graphs that compare energy costs with savings as well as a breakdown of energy use by appliance. BEopt requires a simulation engine, such as DOE-2 or EnergyPlus, to run. The building geometry can include multiple levels,

a garage and other major features of a household. Design options can be left at default values as described in (Hendron and Engebrecht 2010) or set to custom values by the user. Location must also be input to access appropriate weather and solar data—a few weather files are preinstalled, though many more may be downloaded from all over the world.

BEopt may be run in optimization mode in addition to analysis mode. Its optimization feature has been widely used as a modeling tool for costs and benefits of renewable energy options for new homes (Anderson and Christensen 2006). Additionally, it has been used as a tool for finding the optimal solar capacity for ZNE buildings (Horowitz et. al. 2008). To optimize a given building, BEopt analyzes various ways to reduce the energy consumption down to ZNE by changing appliances, insulation and construction materials, building composition, and heating/cooling capacities. Once several ways are determined, the least cost option is selected as the optimal solution. BEopt is capable of customization of economic features as well. Some of these include utility rates, mortgage information, photovoltaic compensation, project lifetime, inflation, discount rate and others.

Chapter 3. Reconciling Consumer and Utility Objectives

In the Residential Solar PV Market

A paper to be submitted to *Applied Energy*

Michael R. Arnold, Nathan G. Johnson

Abstract

Today's energy market is facing large-scale changes that will affect all market players. Near the top of that list is the rapid deployment of residential solar photovoltaic (PV) systems. Yet that growing trend will be influenced multiple competing interests between various stakeholders, namely the utility, consumers and technology providers. This study provides a series of analyses—utility-side, consumer-side, and combined analyses—to understand and evaluate the effect of increases in residential solar PV market penetration. Three urban regions have been selected as study locations—Chicago, Phoenix, Seattle—with simulated load data and solar insolation data at each locality. Various time-of-use pricing schedules are investigated, and the effect of net metering is evaluated to determine the optimal capacity of solar PV and battery storage in a typical residential home. The net residential load profile is scaled to assess system-wide technical and economic figures of merit for the utility with an emphasis on intraday load profiles, ramp rates and electricity sales with increasing solar PV penetration. The combined analysis evaluates the least-cost solar PV system for the consumer and models the associated system-wide effects on the electric grid. Utility revenue was found to drop by 1.2% for every percent PV penetration increase, net metering on a monthly or annual basis improved the cost-effectiveness of solar PV but not battery storage, the removal of net metering policy and usage of an improved the cost-effectiveness of battery storage and increases in solar PV

penetration reduced the system load factor. As expected, Phoenix had the most favorable economic scenario for residential solar PV, primarily due to high solar insolation. The study location—solar insolation and load profile—was also found to affect the time of year at which the largest net negative system load was realized.

Keywords: energy economics, residential solar, solar photovoltaic, net metering, electricity rates, techno-economic optimization

3.1 Introduction

Addressing the societal demand for low-carbon energy is an ongoing challenge that will persist for several decades. It has been suggested that a zero-carbon economy can be realized in the United States by 2050 through a combined approach of changes in technology, policy, economics, business models and consumer behavior (Lovins 2013). Yet that year is far away, and there is much ground to cover. The growing amount of research and industry practice to reduce carbon emissions, however, hints at a trend towards smaller carbon footprints that may one day lead to a zero-carbon society.

This long-term vision has been paralleled with more near-term research emphasizing innovation in renewables design and integration (Nemet et al. 2012, Purohit and Purohit 2010), improving grid stability at high-penetration renewables (Carrasco et al. 2006, Kempton and Tomic 2005, Lund 2005), developing software for integrated building design and building energy systems analysis (Nguyen et al. 2014, Wang et al. 2011), improving energy efficiency in end-use devices (Abramson 1990, Negrão 2011), using thermal energy storage to offset air conditioning loads (Ruddell et al. in review) and evaluating the social, political and economic implications of the low-carbon energy transition (Laird 2013, Miller and Richter 2014, Yun and Steemers 2011). The diversity of

these studies illustrates the many options and complex factors affecting decisions throughout the electric grid from the individual circuit to the larger utility grid.

Household solar photovoltaic (PV) systems are an increasingly common way to offset grid purchases with on-site renewable power generation. For a single residence, rooftop solar PV systems can be sized to generate sufficient energy to fully displace grid purchases on a net basis over a year. Household PV systems commonly produce excess energy that is sent to the grid during sunny periods of the day to compensate for evening hours when no sun is shining and electricity must be used from the grid. The technical and economic effects of rooftop solar are minimal to the grid at low market penetration levels, but are expected to cause grid instability and disrupt utility business models at high penetration levels (Denholm 2007). One of the main concerns is managing the significant drop in the system net load that occurs during high-production hours of the day. Commonly known as the “Duck Curve,” the reduction in net system load during the daytime hours creates a significant ramping request from dispatchable generation at sunset (California ISO 2013). The intermittency in renewables also requires that sufficient dispatchable generation remain online during the day as backup for cloud disruptions in solar PV output. These issues will become more prevalent as distributed generation capacity increases over time.

3.2 Background

Energy system modeling is a broad field with many specializations and technical focus areas based on the type of energy, scale of the system and temporal nature of the design decision to be made. Some models focus on the entire electric grid, others on individual buildings, and yet others on smaller scale energy conversion processes such as

air conditioners, lighting, and cooking. Many of these models are evaluated in isolation, yet the inputs and outputs of each model do affect systems at different spatial and temporal scales.

Models of the electric grid, for example, include data and sub-system models about the transmission and distribution network, renewable and nonrenewable generation assets, resource availability, load profile forecasts and economic forecasts. These models are used to inform capital expansion decisions and specify operational schedules based on metrics such as cost, reliability, and environmental impact. Mathematical representations that describe these metrics are classified as objective functions, and with the aid of modeling and simulation, engineers can quickly alter input parameters and evaluate the objective function to determine the values of inputs that maximize or minimize a quantity to yield an optimal design or decision. Many modeling techniques and software packages are publically or commercially available. No one model is the same, and as a consequent, different models may yield different results or suggested decisions. That should be expected. Even the same mathematical model can result in multiple competing conclusions if different figures of merit or objective functions are selected for optimization (Ostergaard 2009). The challenge of reconciling results pertains directly to studies of transitions in the residential market energy that are influenced by multiple stakeholders, often with competing objectives and models.

Previous studies have examined the costs associated with solar PV installation. There are many costs associated with a PV installation, which are commonly differentiated as initial investment cost and reoccurring annual costs. The initial investment includes the module cost, which accounts for up to 60% of the total cost (IEA 2008), supporting

equipment costs, land cost and a variety of soft costs (Ardani 2014). Annual costs include operation and maintenance and insurance costs. The cash outlay of a PV system to the end-user depends highly on region, largely due to local incentives and government deductions (Reichelstein & Yorston 2012). Past studies have used an installed cost of \$4.00 per watt as of 2010 (Hernández-Moro & Martínez-Duart 2012), which have since fallen further. Leasing a system may also be more cost effective for some buyers. While leasing costs vary by region, they typically have more attractive pricing due to the inclusion of regular maintenance and replacement of key components (Liu et al. 2014).

There is growing body of research that explores the technical and economic implications of solar PV penetration and net metering for consumers and utilities (Mondol et al. 2009). This research has revealed that cost efficiency is necessary for increasing solar PV penetration. Further, the extent of PV penetration and grid rate structure is undoubtedly related (Cai et al. 2013). It has been surmised that the most important factor on utility revenue is the number of solar PV consumers (Pillai et al. 2014). In urban settings, solar PV is not typically viable without tax incentives, rebates and grid rate structures that benefit electricity generation such as net metering. Based on its economic merits, net metering has been shown to be a main cause of the growing solar PV market (Darghouth et al. 2011). Due to such incentives, solar adoption has been growing in recent years, leading many to question its widespread effects at high penetration rates. Studies exploring the challenges of large scale solar PV integration have recognized the need for more research in high penetration scenarios (Katiraei & Aguero 2011).

Modeling approaches and stakeholder engagement efforts that represent and contrast, and perhaps integrate, the perspectives of various parties have proven useful in

facilitating energy planning decisions (Loken 2007, Browne et al. 2010). This article uses a similar approach to contrast the objectives and desired outcomes of residential ratepayers and an electric utility. A single modeling approach is employed using a common set of input data to generate results that include a collection of possible scenarios in low-, medium- and high-penetration solar PV markets. Rather than focusing on one study site, this article offers a comparative analysis between three urban regions using simulated load data and solar insolation data at each locality. Various time-of-use pricing schedules are investigated, and the effect of net metering is evaluated to determine the optimal capacity of solar PV and battery storage in a typical residential home. The residential load profile is scaled to assess system-wide technical and economic figures of merit for the utility.

3.3 Methodological Approach

Electric grid modeling includes expansion planning and production cost modeling for informing mid-term and long-term decisions. Electric utilities use models for capital expansion planning to inform generation, transmission, and distribution capacity decisions. Modeling the addition or upgrade of electricity generation requires well-defined load profile and cost information to inform capital expansion. Production cost modeling complements capital expansion planning assessments to determine how to dispatch available assets to produce the least-cost power. Production cost models are improved by including the techno-economic factors associated to energy use and delivery, in addition to generation, to ensure that equipment can adequately meet the user's needs through the electric grid (Krause et. al. 2010). These two forms of modeling—capital expansion planning and production cost modeling—allow a utility and associated decision makers to

more effectively plan system expansion and operation to address technical, economic, policy and environmental constraints.

Building energy system modeling focuses on determining energy consumption and life cycle costs as a function of building design, occupancy, thermal conditioning, water and energy use. Whole-systems building design uses these and other inputs to provide the user with a great amount of flexibility for modeling different scenarios. Yet in noting that the quality of results depends on the quality of inputs, the input conditions must be researched and well-defined. Optimizing a building energy system goes beyond the selection of power generation, storage or consumption devices in the building. For example, the placement of windows and building orientation can affect power consumption—e.g., large southward facing windows can reduce the use of heating systems because more sunlight enters and warms the building. Some software packages allow users to evaluate and contrast the effects of building design decisions and equipment decisions on technical, environmental and economic metrics.

3.3.1 Household Electric Load Profile Creation

This article utilizes the Building Energy Optimization (BEopt) tool to simulate and generate load and solar resource profiles. BEopt was created to assist in the design of zero net energy (ZNE) buildings (Christensen 2010). ZNE buildings are defined as those which produce as much electricity as they consume. To this end, BEopt provides mechanisms to evaluate whole-building energy savings based on building size and orientation, a suite of energy use devices, occupancy data, location and building materials composition and structure. Although BEopt can be used for new and existing construction, it is commonly employed as modeling tool to describe the costs and benefits of renewable energy options

for new residential construction (Anderson and Christensen 2006, Horowitz et. al. 2008). BEopt reports total and hourly energy usage within an intuitive graphical user interface (GUI) that uses an underlying simulation engine, such as EnergyPlus, for building energy calculations.

Building options in BEopt are set to default industry values as listed in the Building America house simulation protocols (Hendron and Engebrecht 2010), with a few areas of note or deviation: the house has a gas water heater and gas cooking range, an electric clothes dryer and is spaced 20 feet apart from neighboring households.

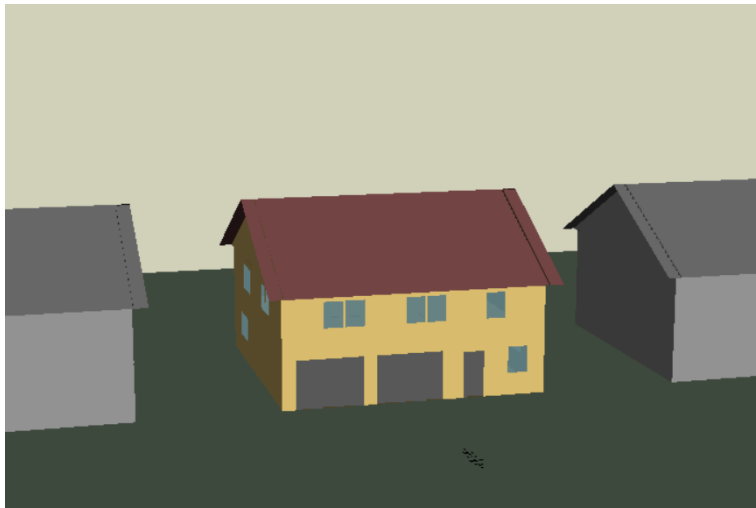


Figure 3.1. Household Visualization in BEopt.

The house for simulation is a two story, square home with 38 ft. by 38 ft. dimensions that equates to a total of 2388 ft² after subtracting the garage space of 25 ft. by 20 ft. on the first floor (Figure 3.1). According to the U.S. Census Bureau, this square footage is near the national average of 2,392 (2010).

A BEopt model is run for three separate locations: Chicago (41° 59' N, 87° 54' W), Phoenix (33° 26' N, 112° 1' W) and Seattle (47° 32' N, 122° 18' W) using BEopt's predefined locational data. These three locations are chosen due to their difference in solar

insolation, climate, precipitation and latitude. While Seattle and Chicago have similar amounts of solar insolation through most months of the year, it is thought that Seattle's rainy season will have an interesting effect on solar insolation during several months, providing implications regarding utility operating reserve. Hourly time series outputs taken from BEopt and input into HOMER include the hourly residential load (kW) and solar global horizontal insolation (kW/m²). HOMER includes algorithms to generate synthetic solar data, and these had to be overridden using the hourly data from BEopt to maintain data consistency across the two modeling packages.

Figure 3.2 summarizes the annual solar profile for each study location using a heat map to visualize the solar insolation in all 8760 hours over a one-year period. The solar insolation profiles of Chicago and Seattle are fairly similar, with high yet intermittent solar radiation during the summer months and low solar radiation during the winter months. Seattle, however, experiences a much larger drop in solar radiation during November, December and January. Phoenix receives solar radiation for more hours of the day during the winter due to its low latitude, and has a stronger and more consistent daily solar profile over the summer and winter months when compared to Chicago or Seattle profiles.

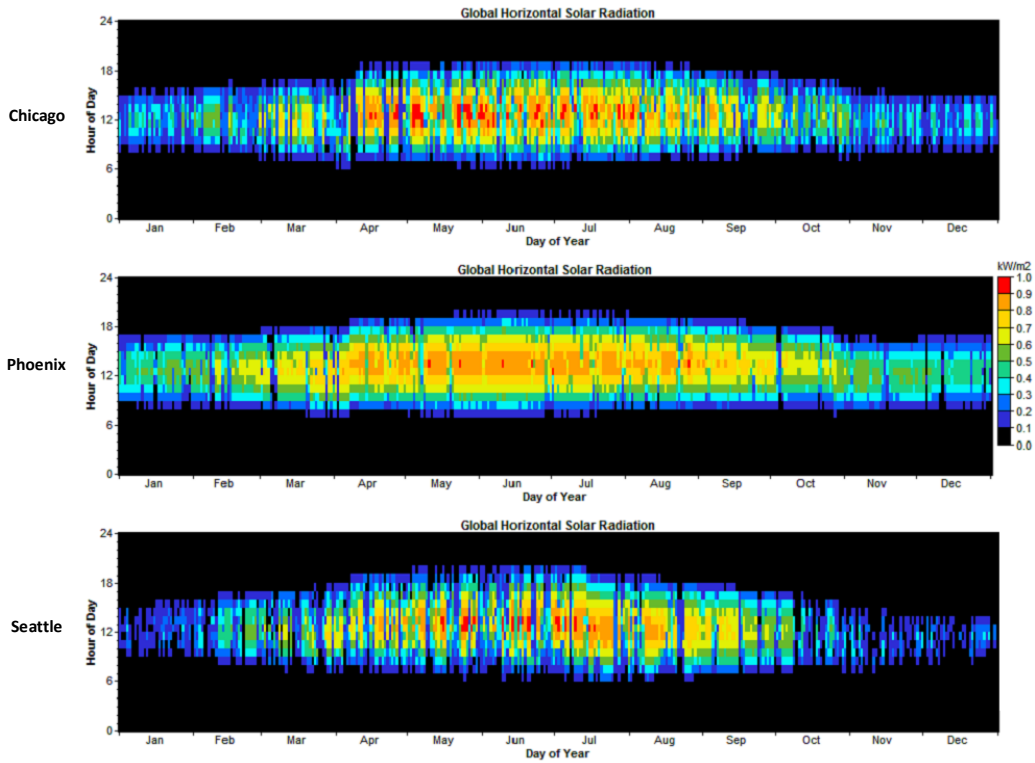


Figure 3.2. Hourly Global Horizontal Solar Radiation at Study Locations.

There are several distinct differences in the household energy usage modeled for each study location (Table 3.1). Phoenix has a high average and peak power demand, as compared to Chicago and Seattle, due to the increased need for air conditioning in the warm climate. Households in Chicago and Seattle have a similar total energy usage but Chicago experiences a higher peak. The minimum load is similar across all locations, which is an artifact of using the same BEopt model input parameters for each study location, and noting that low demand of cooling systems in the winter months.

Table 3.1. Household Energy Usage Summary.

Location	Average (kW)	Peak (kW)	Min (kW)	Total (kWh)
Chicago	1.00	2.84	0.41	8,765
Phoenix	1.57	5.29	0.44	13,750
Seattle	0.90	2.09	0.41	7,887

3.3.2 Household Solar PV System Sizing and Aggregate Utility Effects

This paper uses the Hybrid Optimization Model for Electric Renewables (HOMER®) to compare power system configurations for systems topology selection and system sizing. HOMER models the physical behavior of a power system and quantifies the total cost of installing and operating the system over its lifespan. Its graphical user interface allows users to interactively compare design options on their technical and economic merits. HOMER performs three principle tasks: simulation, optimization, and sensitivity analysis. Chronological simulations are completed over a one-year period for the range of micro-grid systems specified by the user. HOMER then identifies the optimal system size and control strategy with the lowest net present cost. Sensitivity analysis is used to test the effect of model assumptions and input parameters on system robustness. HOMER has been used in selecting optimum components for hybrid energy systems (Fulzele & Dutt 2012). It has also been used in conjunction with optimization algorithms, such as particle swarm optimization to find the optimal amount of solar to install (Hafez & Bhattacharya 2012). Although HOMER was developed primarily for use in planning off-grid micro-grid power systems, it can be used to simulate residential-scale grid-connected systems and model a simplified representation of the electric grid as a single electric circuit to calculate load and economic statistics (Johnson et al. 2011). A more detailed discussion of HOMER algorithms and functionality is found in (Lambert 2006).

HOMER is first used to create the household net load profile for the minimum and maximum amount of solar PV capacity. The maximum allowed PV system size is determined using (Eq. 3.1). The capacity factor is taken from HOMER and annual total energy usage is taken from the annual load data created in BEopt and used in HOMER.

The scaling factor of 120% is commonly used by utilities to define the limit on PV system size under which net metering is permitted. The maximum permitted residential PV array capacities are equated as 8.64 kW for Chicago, 9.06 kW for Phoenix and 8.76 kW for Seattle. The capacities are similar because the greater total energy use in Phoenix is offset by a greater capacity factor, meaning that a solar PV panel installed in Phoenix will output more energy annually than the same panel installed in Chicago or Seattle.

$$PV_{max} = CF(120\% E_{tot,y}) \quad (3.1)$$

CF = capacity factor (%)

$E_{tot,y}$ = total annual energy usage (kWh)

Residential load profile simulations and energy expenditures are completed for each study location using the following model input parameters:

- Solar PV array—The rooftop array is mounted at a slope equivalent to the latitude in each study site to achieve maximum energy output over the year. Shading affects and temperature effects are not considered. A derating factor of 80% is selected to account for soiling losses and other discrepancies between the rated power output and installed power output. Rooftop array capacities are evaluated at 0%, 25%, 50%, 75%, and 100% of the maximum capacity permitted in each study site.
- Inverter—The DC-to-AC conversion efficiency is assumed to be a constant 90%. Inverter sizes are evaluated at capacities equivalent to the rooftop array in each study site.

- Battery—A Surrrette 4KS25P battery is used with a nominal 4V and 1,900 Ah capacity. Initial costs are assumed at \$1,200, replacement costs at \$800, and operation and maintenance costs at \$40 / battery / yr.
- System costs—System costs are modeled as single scalable quantity based upon the PV array size. Cost assumptions include an installed system capital cost of \$3.00 per W after rebates and incentives, and an annual operating and maintenance cost equated at 1% of the installed system capital cost. The system lifetime is modeled at 20 years with inverter replacement at 10 years that is included in the system capital cost.
- Grid electric price—A grid connection fee of \$15 is charged each month. Table 3.1 provides a summary of three time-of-use (TOU) cases simulated using peak power pricing between 1pm and 7pm. Case 1 has no TOU increase, Case 2 has a 50% increase and Case 3 has a 100% increase in the cost of electricity. The rates in Table 3.2 include all taxes and fees.
- Net metering—Net metering was evaluated in three ways: no net metering, net metering calculated monthly and net metering calculated annually. A flat sellback rate of \$0.03/kWh was specified across all models to reflect the sale of any net excess generation from the household PV array.
- Price escalation—Although HOMER cannot evaluate grid price escalation over the project lifetime, increases in grid cost can be modeled implicitly using a negative annual real interest rate and compensating for the effect when selecting equipment replacement costs that will be encumbered over the system lifetime. A grid price escalation of 3% per annum is used.

Table 3.2. Grid Rate Structures (\$/kWh).

Rate period	No TOU	TOU	
	Case 1	Case 2	Case 3
Non-summer	0.12	0.12	0.12
Summer off-peak	0.16	0.16	0.16
Summer peak	0.16	0.24	0.32

The utility-scale effects of residential solar PV penetration are calculated by scaling the individual residential load profile by 500,000 in each simulation (Eq. 3.2).

$$P_{utility} = P_{res} \times N_h \times (1 - PV_{pen}) + P_{net} \times N_h \times PV_{pen} \quad (3.2)$$

$P_{utility}$ = utility side power draw (kW)

P_{res} = residential power use (kW)

N_h = number of households (unit less)

PV_{pen} = PV penetration (%)

P_{net} = consumer side net power draw with 100% PV capacity (kW)

Utility-scale effects are explored by assuming that homes installing solar PV use the maximum allowed capacity as calculated by Eq. 3.1. The hourly system load profile and economic metrics are evaluated for residential PV adoption rates of 0%, 5%, 10%, 15%, 20% and 25%. January, April, July and October are selected to demonstrate the effects on the system load profile over various parts of the year.

A combined analysis follows the residential analysis and utility analysis by relaxing the assumption that consumers install maximum PV capacity. Rather, consumers are modeled as rational agents that seek to minimize their energy expenditures by selecting the

least-cost combination of solar PV capacity and batteries, or installing no solar PV or batteries. Analysis is again completed for each grid rate structure and net metering policy.

3.4 Results and Analysis

3.4.1 Utility Implications

The average hourly net load data described by Figure 3.3 exhibits the “Duck Curve” behavior at higher PV penetration, as expected. The load profiles shown in each month are equated as an average of the hourly load profile of each day in a month. Net load profile curves overlap in the early and late hours of the day due to a lack of sunlight. Phoenix displays no negative net load in July—peak solar insolation in all study sides—due to the high usage of electrically power central air conditioning units. Chicago and Seattle, on the other hand sees their biggest peak in January due to additional lighting loads not needed in other months with more daylight. There is a minimal system-wide effect of residential PV in Seattle during the month of January due to the largely overcast sky. Chicago and Seattle have their lowest minimum net load in July. By contrast, Phoenix has its minimum in April due to the high solar insolation and relatively minimal cooling load as compared to July in the same location. The maximum ramp rate that the utility must meet for each case may be inferred from Figure 3.3 where the slope of the line is greatest. These ramp rates occur at either 4:00 pm or 5:00 pm for all cases. Duck charts such as the ones in Figure 3.3 show how ramp rates drastically change solar PV penetration increases, potentially causing scheduling and loading issues for the utility generation fleet.

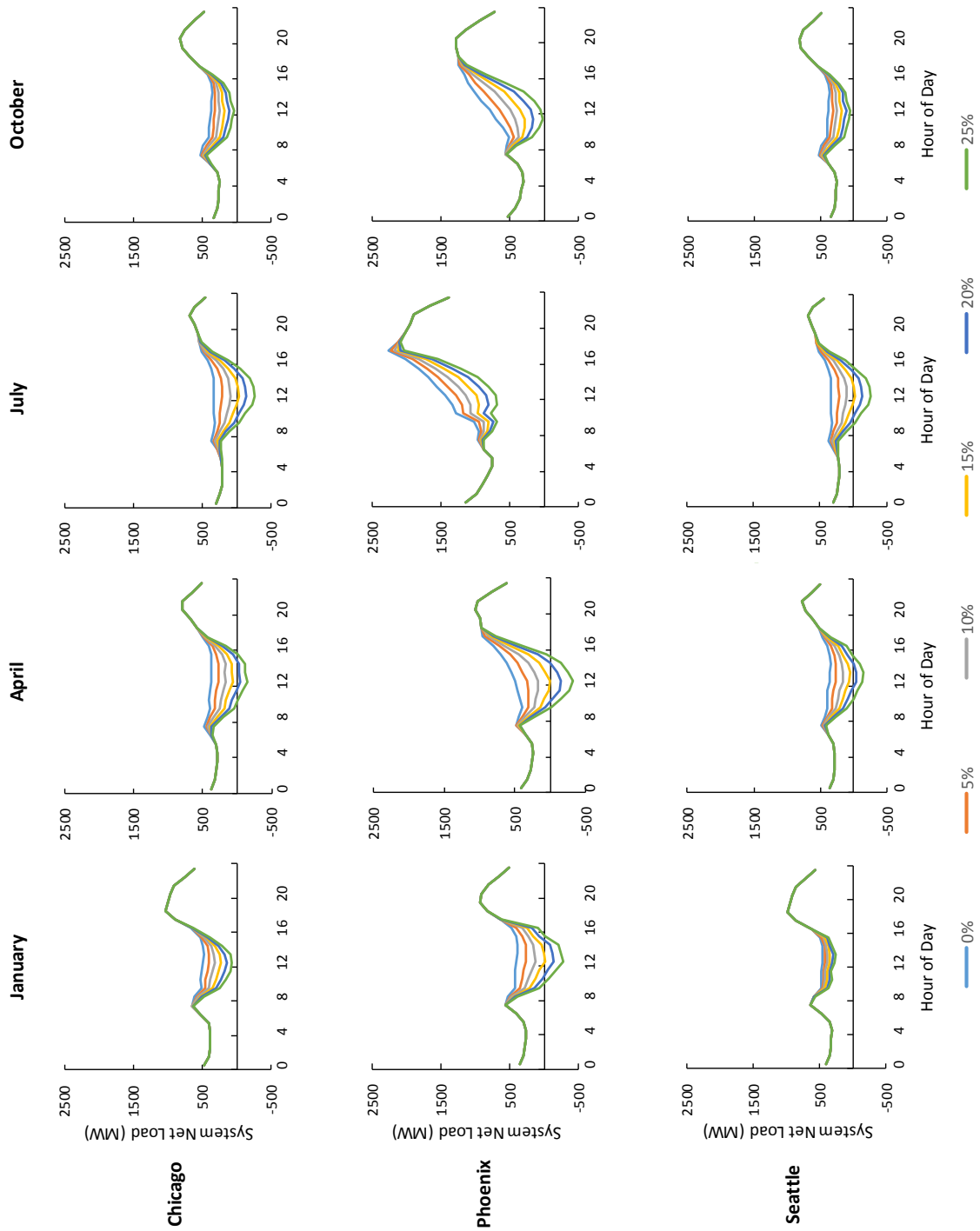


Figure 3.3. System Net Load Curves at Selected Solar PV Market Penetration Levels.

Massive amounts of excess generation from residential solar PV systems can overload and congest the distribution grid. Table 3.3 provides the level of market

penetration at which residential solar causes a negative load for the residential portion of the system load in various months of the year. This was equated from the average daily load profile in each month as described earlier. Negative system loads occur at lower PV penetration rates in locations and times of year with high solar insolation and low cooling loads—as seen in January and April in Phoenix, or July in Chicago and Seattle. In Seattle, January is the month of the year least likely to experience negative system loads due to persistent overcast skies in that month. But in Phoenix, July is the month of the year least likely to experience negative system loads due to the high demand for air conditioning. The difference between months in a location such as Phoenix display how seasonal changes greatly affect the energy dispatch schedule of a utility. Those regions which more easily reach a negative net load need more robust infrastructure to deal with excess power generation.

Table 3.3. Residential Market PV Penetration that Produces Negative System Load.

Location	January	April	July	October
Chicago	29%	18%	14%	28%
Phoenix	15%	15%	49%	27%
Seattle	61%	18%	14%	28%

The effects of PV penetration on average power, peak power, minimum power, total energy and load factor are summarized in Table 3.4. Rooftop solar penetration was seen to have a negligible effect on the peak system load in Seattle, but was seen to decrease the peak in Chicago and Phoenix (Figure 3.4). PV penetration changed the load factor similarly for all locations in this study. In summary, changes in PV penetration affected all metrics—except the peak power—similarly across the study locations.

Table 3.4. System Effects of Solar PV Market Penetration.

Location		Solar PV Market Penetration					
		0%	5%	10%	15%	20%	25%
Chicago	Average (MW)	500	470	440	410	380	350
	Peak (MW)	1,420	1,395	1,371	1,346	1,323	1,321
	Min (MW)	206	44	-121	-287	-452	-617
	Total (MWh)	4,382,698	4,119,481	3,856,264	3,593,047	3,329,830	3,066,613
	Load Factor	0.35	0.34	0.32	0.3	0.29	0.27
Phoenix	Average (MW)	785	742	700	657	615	572
	Peak (MW)	2,644	2,600	2,556	2,548	2,543	2,538
	Min (MW)	221	123	-37	-199	-381	-563
	Total (MWh)	6,874,944	6,502,892	6,130,841	5,758,790	5,386,739	5,014,688
	Load Factor	0.3	0.29	0.27	0.26	0.24	0.23
Seattle	Average (MW)	450	426	401	377	353	328
	Peak (MW)	1,046	1,045	1,045	1,045	1,045	1,045
	Min (MW)	206	56	-98	-252	-406	-560
	Total (MWh)	3,943,261	3,729,914	3,516,567	3,303,221	3,089,874	2,876,528
	Load Factor	0.43	0.41	0.38	0.36	0.34	0.31

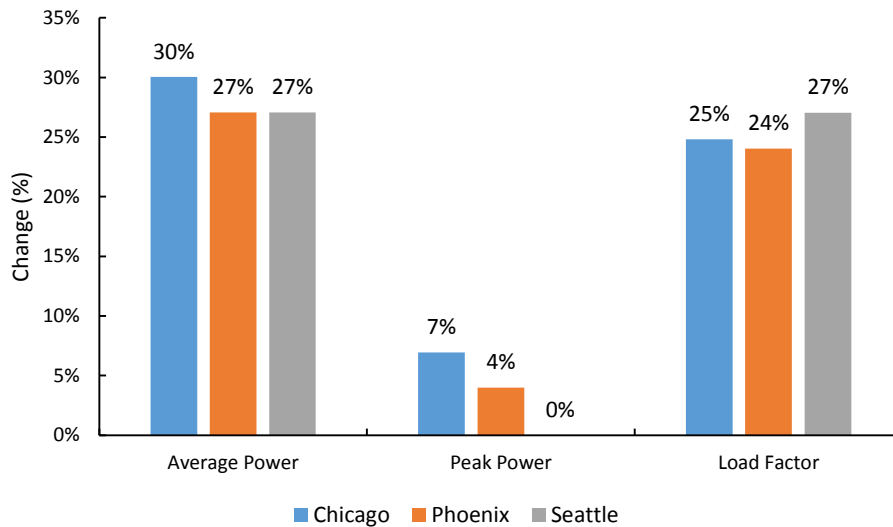


Figure 3.4. Relative Effects of Solar PV on Electric Grid at 25% Penetration.

The data in Table 3.5 describes the annual revenue for a utility under the previously simulated conditions. Data in the table was selected for simulations of net metering on a monthly basis, which is the common time period for residential net metering agreements.

As expected, increased PV penetration decreases utility revenue, and increases in on-peak power price increased utility revenue. It is worth noting, however, that raising the on-peak price does not mitigate the effects of increased PV penetration. The average difference in revenue for Chicago, Phoenix and Seattle from 0% to 25% PV penetration is 32%, 26% and 31%, respectively. This means that on average, the utility revenue dropped 1.2% for every percent PV penetration increase. Also, the monthly connection fee of \$15 per resident contributed 12% of total revenue at 0% penetration and 16% of revenue at 25% penetration. Thus, for every 5% increase in PV penetration, the connection fee contributes 1% more to annual revenue.

Table 3.5. Utility Annual Revenue as Percentage of Solar PV Adoption at Max Capacity.

Location	On-Peak Price (\$/kWh)	Utility Revenue (\$ 000,000)					
		0%	5%	10%	15%	20%	25%
Chicago	0.16	671	635	510	564	528	492
	0.24	706	669	536	587	547	507
	0.32	740	702	563	610	566	523
Phoenix	0.16	1,028	1,008	958	908	858	808
	0.24	1,157	1,011	1,046	990	935	879
	0.32	1,256	1,105	1,134	1,072	1,011	950
Seattle	0.16	608	488	548	539	489	459
	0.24	630	507	564	531	498	464
	0.32	653	526	580	543	506	470

3.4.2 Household Implications

The optimal PV system sizes were determined for each location with net metering (monthly/annually) and without net metering at the three on-peak grid prices (Table 3.6). The optimal size is the least-cost option for the consumer, and may include no solar PV. Of all the capacities evaluated, the largest systems are in Phoenix due to the excellent solar insolation resource. Without net metering, PV is not a viable option in Seattle due to the

low amount of solar insolation. However, with net metering, using a small amount of solar PV can be cost effective in places such as Seattle. This illustrates how net metering has the capability of greatly increasing the viability of PV because it credits excess generation in a one-to-one trade for use later when PV generation cannot meet the household load. Higher on peak prices also contributed to cost effective PV. This is due to highest solar insolation and energy prices typically occurring at the same time.

Table 3.6. Optimal PV Capacities for the Consumer.

Location	Peak Price (\$/kWh)	Optimal PV Capacity	
		No Net Metering	Net Metering (Monthly/Annually)
Chicago	0.16	10%	50%
	0.24	15%	55%
	0.32	20%	60%
Phoenix	0.16	35%	80%
	0.24	40%	85%
	0.32	45%	90%
Seattle	0.16	5%	10%
	0.24	10%	30%
	0.32	15%	35%

The levelized cost of energy (LCOE) (Eq. 3.3) paid by the consumer is given in Figure 3.5 for the 20-year simulation of each grid rate structure, net metering policy and solar PV capacity. A larger data marker is used to show the least-cost PV capacity for each case. Monthly and annual net metering had a negligible difference in the consumer-side economics due to the limitation on system size and low sellback rate of \$0.03/kWh.

$$LCOE = \frac{C_{ann,tot}}{E_{ann,tot}} \quad (3.3)$$

$C_{ann,tot}$ = total annual cost of energy (\$/kWh)

$E_{ann,tot}$ = total annual energy (kWh)

Without net metering, the optimal system size in Chicago and Seattle was below 20% of max because of limited energy usage during peak hours and a low sellback that indicates there is no economic justification for the consumer to install solar panels that produce any excess generation. The optimal capacity was higher in Phoenix than Chicago and Seattle due to higher loads and solar insolation levels. With net metering, the cost-effectiveness of solar PV increases in all scenarios—as seen in the reduction in LCOE values on the graphed curves with net metering. Optimal capacities increased in nearly all cases, with the largest size PV array being in Phoenix. The levelized cost of energy has an inverse relationship with the solar insolation, and yields the lowest LCOE in Phoenix, followed by Chicago and then Seattle. Higher peak prices also contributed to a slight increase in optimal PV array size to ensure that on peak electricity loads are met without utility purchases. In most of the cases, the pricing curves converge at higher PV capacities. This indicates that energy pricing has less influence on LCOE at high install capacities because solar PV costs contribute a larger portion of total invested cost relative to hourly energy pricing.

It is interesting to note that, even without net metering, there is little difference in the LCOE between installed arrays at 0% and 100% of max capacity. This indicates that residents living in the Phoenix area could make a choice to install solar PV systems for personal or environmental reasons and experience little, if any, impact on their average cost of energy. With the option of net metering in Seattle, the LCOE does not increase at the rate it does without net metering. The difference in optimal PV capacity between using net metering and not for Seattle is much smaller than Chicago or Phoenix due to the small

amount of solar insolation. Thus, higher insolation translates into net metering having a larger effect on optimal PV capacities.

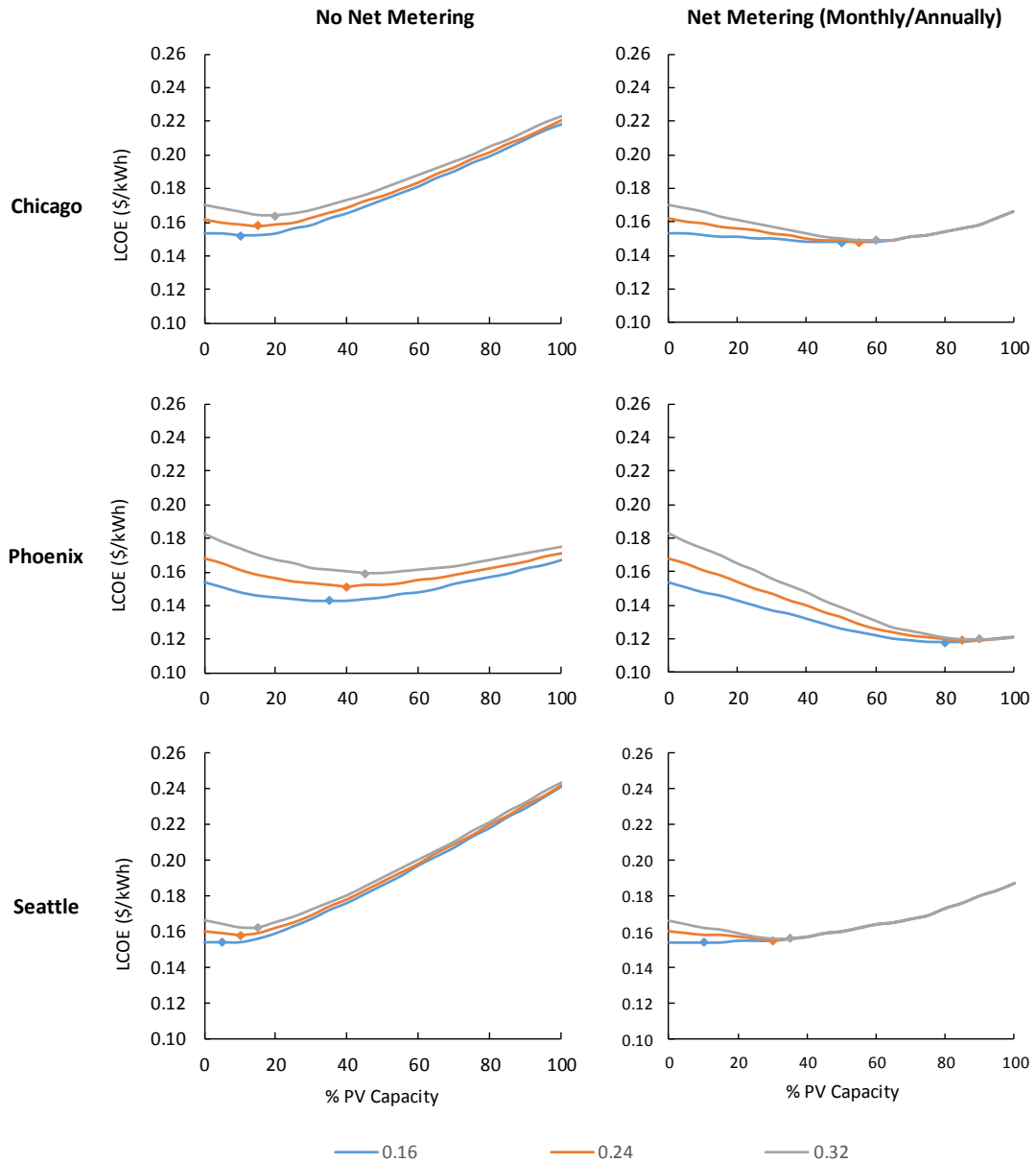


Figure 3.5. Levelized Cost of Energy for Grid Rate Structures and PV System Sizes.

The household analysis was extended by modeling the use of batteries in the home, with or without a PV array. HOMER simulations were completed with battery costs ranging from 0% to 100% of the component's assumed cost. Figure 3.6 provides a

graphical representation of the optimal system type—set of power system components with least cost energy—for each study location. Batteries were only cost-effective in cases without net metering, at a high on-peak grid price and at a greatly reduced battery cost. Yet even if the battery is free, it may not be cost effective since the efficiency losses increase the cost of energy cycled through the battery (Eq. 3.4). In scenarios with higher on-peak grid prices, however, a battery can be useful for storing low-cost energy from off-peak times and discharge it during higher on-peak times, if the battery capital cost is sufficiently low to warrant acquisition. Batteries were never a cost-effective option in any case using monthly or annual net metering. Under net metering policy, consumers can use the grid as a “lossless zero-cost battery” and have no economic justification to install storage, although ancillary benefits such as backup power may be desired. Batteries had the most favorable business case in Phoenix because solar PV could not fully meet electric loads during summer peak hours.

$$C_{e,o} = \frac{C_{e,i}}{\eta_{bat}\eta_{inv}\eta_{rec}} \quad (3.4)$$

$C_{e,o}$ = cost of energy taken out of the battery (\$/kWh)

$C_{e,i}$ = cost of energy put into the battery (\$/kWh)

η_{bat} = battery efficiency (%)

η_{inv} = inverter efficiency (%)

η_{rec} = rectifier efficiency (%)

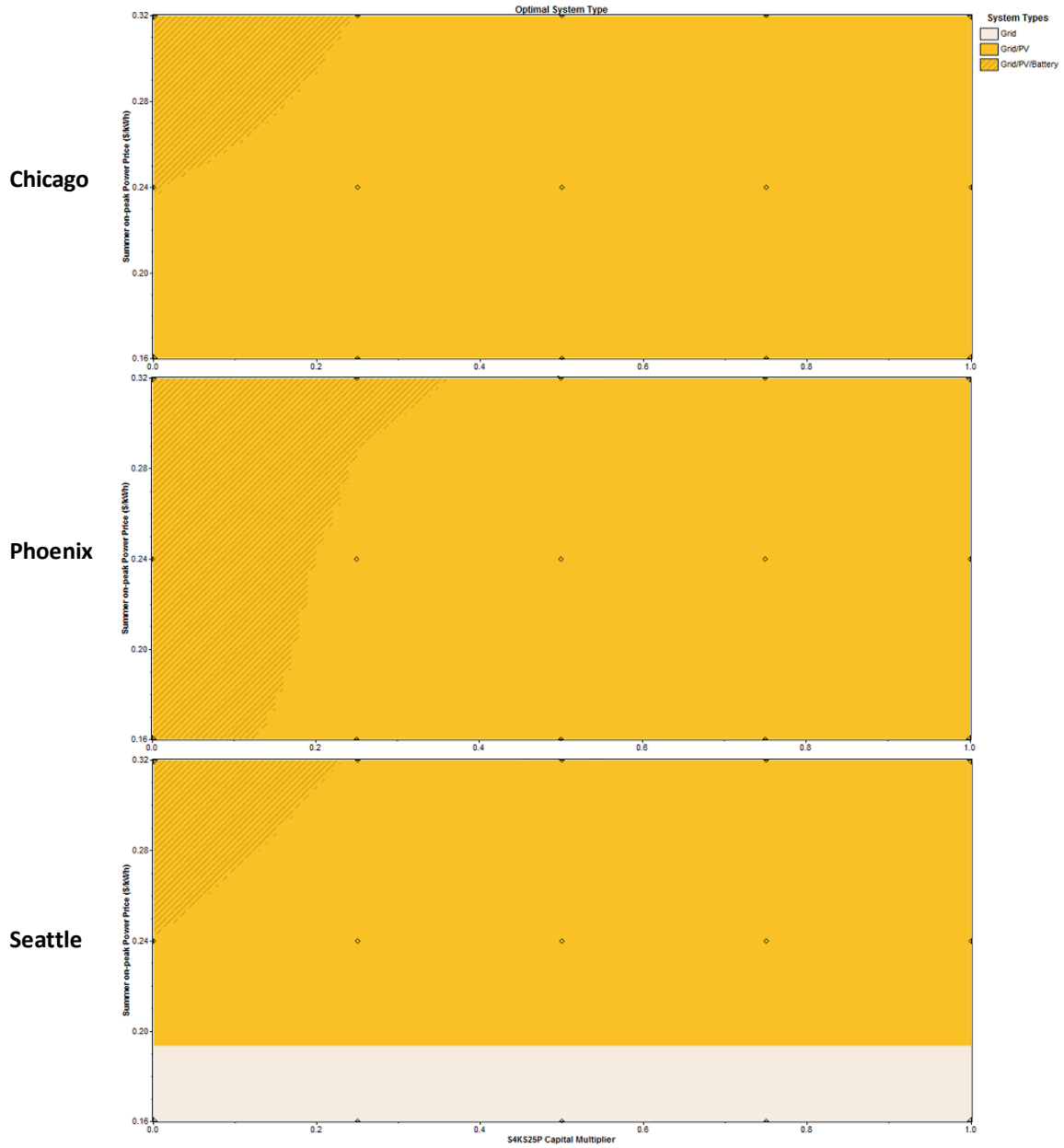


Figure 3.6. Optimal Power System Configuration Considering Batteries.

3.4.3 Combined Analysis

The combined analysis is predicated on the assumptions that the decision to install PV and batteries lies solely in the hands of the consumer, the consumer makes a decision based on their own economic interests to reduce expenditures on energy and energy

technologies, all consumers can financially and legally install any amount of PV and batteries and all consumers make the same decision to select the least cost option for their locality. Monthly net metering is used for the analysis. For Seattle, there is a negligible difference in the consumer's LCOE between 0% and 25% solar capacity, and so the curves generated in Figure 3.7 for Seattle have been calculated using 25% solar capacity for easier visualization. The curves were calculated for Chicago using 50% solar capacity and Phoenix using 75% solar capacity.

The decrease in revenue for the utility, on average, is 1.1% for every percent of system-wide PV solar capacity that is installed in the combined analysis (Table 3.7), which is very similar to the 1.2% drop in revenue for every percent of residential PV consumers that adopted solar at max capacity in the utility implications analysis (Table 3.5). Table 3.7 includes the monthly connection fee. A utility in the Chicago area would experience a drop of 57% in revenue if solar PV was installed at 50% of max capacity, Phoenix a drop of 74% in revenue for 75% of max solar PV capacity and Seattle a drop of 30% in revenue for 25% of max solar PV. As expected, utility revenue drops with increasing amounts of residential solar PV, but dropped at a greater rate when higher peak prices were simulated. Simulations with higher peak prices created a greater percentile drop in utility revenue because the utility would be selling less energy during high price hours as residential consumers installed more solar PV.

Table 3.7. Utility Annual Revenue as Percentage of System-wide Solar PV Capacity.

Location	On-Peak Price (\$/kWh)	Utility Revenue (\$ 000,000)	
		0%	100%
Chicago	0.16	671	352
	0.24	706	355
	0.32	740	357
Phoenix	0.16	1,058	348
	0.24	1,157	363
	0.32	1,256	378
Seattle	0.16	608	459
	0.24	630	464
	0.32	653	469

The effect of installing various amounts of PV capacity (25%, 50%, and 75%) on utility net load is illustrated in Figure 3.7. As expected, there is a greater effect on net load in areas with higher installed capacity—i.e., Phoenix. The cooling load demand seen during the morning and midday hours in Phoenix in July is largely offset but is minimally affected at peak load hours between 2pm and 4pm. Based on Figure 3.7, the amount of negative net load on the grid would be extreme for such an installed capacity. The net loads are lowest in Phoenix during April and October, when the cooling load is low and solar insolation is still high. The difference in net loads for Seattle further illustrates the highly variant levels of solar insolation received between the winter and summer months. It is worth noting that even Seattle, the location shown to have the lowest amount of solar insolation, and having the lowest installed PV capacity (25%), still caused a negative net load on the grid for two of the four months portrayed in the illustrations. Chicago has the most regular net load profile across the year, with very little difference in its peak and minimum loads. Ramp rates—in absolute or relative metrics—may be inferred from Figure 3.7. Locations with high solar insolation are likely to have more technical issues regarding grid overloading

because more consumers are likely to install PV. Conversely, locations with low solar insolation such as Seattle have a much less chance of having technical issues because consumers would install small solar PV arrays. The monthly connection fee contributed 13% of annual revenue at 0% installed capacity but contributed 30% of revenue at 100% capacity, noting that increasing the connection fee may be a mechanism to recoup lost revenue.

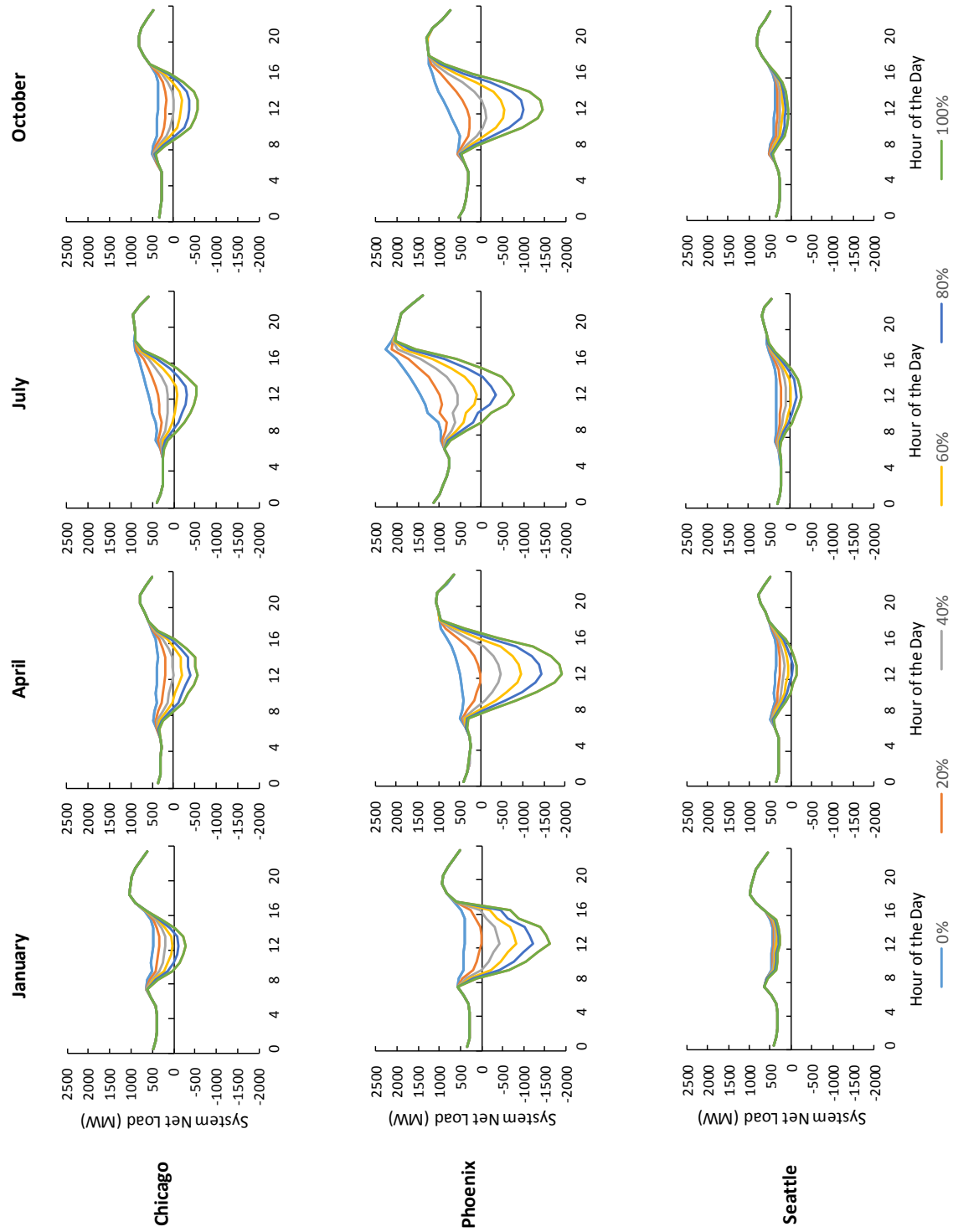


Figure 3.7. System Net Load Curves at Optimal Rooftop Capacity for Residences.

3.5 Discussion and Conclusions

This study examined the implications of installing high penetration solar PV across several locations with different load and solar insolation profiles. Simulated hourly load and solar insolation data was used in a comparative analysis of different levels of solar PV penetration and grid rate structures on technical and economic merits. Optimal scenarios were identified and evaluated for the consumer, the utility and a combined analysis that considered objectives of both stakeholders. Differences in system-wide net load effects for each study location imply that solar PV penetration will affect the separate regions differently. From this it can be inferred that the technical, economic and policy components of integrated resource planning need to be evaluated within the context of local climate, weather patterns, energy usage behaviors, load profile and grid rate structures. Some examples are summarized below:

- The optimal residential power system configuration—solar PV and/or battery storage—and component capacities differed for each location.
- High electric loads required to cool buildings in Phoenix lead to larger peak demands and greater price-performance for solar PV during the warmer midday hours.
- A solar only system was more cost-effective than a solar-battery system in nearly all scenarios investigated. The cost-effectiveness of battery storage increased as battery prices dropped by 65% to 100% and TOU peak prices increased. Phoenix had the most favorable economic conditions for battery storage due to significant summer cooling loads, whereas Seattle and Chicago had similar market opportunities with almost no market advantage for battery storage.

- The largest net negative system loads occurred in April for Phoenix but in July for Chicago and Seattle.
- Overcast days in Phoenix may lead to large swings in the net load that would require utility generation fleet with sufficient operating reserve and ramp rate capacity to address sudden drops in residential solar PV output. Ramp rate requirements are less in Chicago and least in Seattle.

The amount of PV penetration that would cause a negative net load on the grid was highly dependent on location. Simulating and forecasting how solar PV penetration rates may affect intraday and intrahour net load profiles can help utilities plan for inherent problems associated to renewable intermittency. Further, simulating the effects of PV penetration on average power, peak power, minimum power, total energy and load factor is also a useful way for utilities to plan for future effects of solar PV at an aggregate level. These effects are again largely dependent on the solar insolation and energy usage dynamics of a specific region. In all locations, a solar PV penetration of 25% was found to create a negative residential net system, suggesting that utilities may be experience dispatch and operating reserve challenges, or congestion challenges at the feeder or substation level in subdivisions of a city with higher penetration renewables.

This study also provides insight into how PV penetration affects utility revenue. Losses in revenue due to increases in solar PV capacity are beginning to cause disruptions in utility business models. The primary tactics to compensate for a drop in revenue is to raise prices—increase electricity prices (\$/kWh)—or add new revenue streams—tariff for having rooftop solar or an increase in the connection fee. Another option is to change the shape of the market, such as by altering net metering policy. The removal of net metering—

monthly or annual—was found to have the most significant impact on the cost-effectiveness of solar PV and, therefore, on the capacity installed by the consumer and the effect on the utility’s revenue. Yet, the country-wide shift towards advanced metering infrastructure (AMI) or smart meters is an enabler of net metering, and the significant economic and human resource allocation for this effort may lead stakeholders to other courses of action, particularly since AMI technologies allow real time communication between consumer and utility, thereby improving demand response capabilities and more real-time communication of pricing. Additionally, utility companies could recoup lost revenue by implementing a monthly tariff to the consumer or rooftop PV leasing agency, or by instating a demand charge.

Some additional general findings are summarized:

- Results in this study showed little difference between monthly and annual net metering. This was largely due to the low sellback price.
- Solar PV penetration had little effect on peak power draw. Therefore a utility’s generation fleet must be maintained and online to provide peak power requirements despite a reduction in capacity factor due to operating at lower loads as net load drops.
- Demand response capabilities may serve a greater role in the residential energy market as system-wide operating reserve capacity requirements increase with increases in renewable penetration.
- Net metering was shown to decrease the cost-effectiveness of batteries due in part to their efficiency losses and those associated with a converter. For a grid-connected system, the grid can be effectively characterized as a “no cost lossless battery.”

Reaching a zero-carbon emission economy is a challenge that will require innovative technology and techniques to address energy consumption. Our society is trending towards smaller carbon footprints, causing a change in policy, economics, business models and consumer behavior. This study works toward that goal by emphasizing the design and integration of renewables, providing insight on grid stability at high-penetration renewables, exploring software for production cost modeling and expansion planning, and discussing the implications of a low-carbon energy transition. With PV systems becoming a more popular way to offset grid purchases, sizing equipment based on the optimal choice is more important than ever to ensure economic efficiency in the short-term and grid stability in the long term. This study has attempted to analyze both dynamics to help inform future economic and policy decisions, as these issues become more prevalent over time.

There are a few limitations of this study that are common to all modeling and simulation approaches. As with all modeling studies, it is important to remember that models are but one representation of what might happen, not what will actually happen. This is the primary reason for studying multiple locations across multiple scenarios. The models used in this study used as much real world data as was feasible, making the fewest assumptions possible to ensure reliable results. The low energy sellback resulted in no significant difference between annual and monthly net metering. This may not necessarily be the case for all situations, as pricing structures vary highly depending on location. Each component had its pricing and efficiencies implied based on current technology and availability, which will change over time and across locations. This is important to take into consideration when reviewing some of the conclusions. Additionally, it was assumed

that all consumers would make a decision to choose the least cost option for solar PV installments and that everyone could do so. Of course this is not the case, but it is important to understand the effects of PV installations and how net energy load is affected by different amounts of PV penetration.

Areas of future work include analyzing the utility-side effect of high-penetration rooftop solar on utility emissions and economics from running nonrenewable generation at low loads due to operating reserve requirements, evaluating the techno-economic performance of other battery chemistries, developing load management scenarios to smooth residential load profiles and provide system-wide operating reserve at reduced cost to consumers and utilities, expanding the analysis to include more case study locations and evaluating the consumer-side and utility-side effects of additional grid rate structures such as daily or hourly net metering.

References

- Abramson, D. S., Turiel, I., & Heydari, A. (1990). Analysis of refrigerator-freezer design and energy efficiency by computer modeling: DOE perspective. *ASHRAE Transactions*, 96(Part I), 1354-1358.
- Anderson, R., Christensen, C., & Horowitz S. (2008). Searching for the Optimal Mix of Solar and Efficiency in Zero Net Energy Buildings. *National Renewable Energy Laboratory*.
- Anderson, R., Horowitz, S., Courtney, A., & Spencer, J. (2006). BEopt software for building energy optimization: features and capabilities.
- Archana, N., & Sumathi, S. (2012). Unit Commitment and Economic Load Dispatch using Self Adaptive Differential Evolution. *WSEAS Transactions on Power Systems*, 7(4).
- Ardani, K. (2014). Benchmarking Non-Hardware Balance-of-System (Soft) Costs for US Photovoltaic Systems Using a Bottom-Up Approach and Installer Survey. *National Renewable Energy Laboratory*.
- Augenbroe, G., Wilde, P. D., Moon, H. J., & Malkawi, A. (2004). An interoperability workbench for design analysis integration. *Energy and Buildings*, 36(8), 737-748.
- BEopt. (n.d.). *Features*. Retrieved July 13, 2014, from <https://beopt.nrel.gov/>
- BlueFin® Products Spirae. (n.d.). *BlueFin® Products Spirae*. Retrieved July 13, 2014, from <http://www.spirae.com/products/blue-fin-platform>
- Browne, D., O'Regan, B., & Moles, R. (2010). Use of multi-criteria decision analysis to explore alternative domestic energy and electricity policy scenarios in an Irish city-region. *Energy*, 35(2), 518-528.
- Building Energy Use and Cost Analysis Tool. (n.d.). *Overview*. Retrieved July 13, 2014, from <http://doe2.com/DOE2/index.html>
- Bushby, S. T., Galler, M. A., Ferretti, N. M., & Park, C. (2010). The Virtual Cybernetic Building Testbed--A Building Emulator. *ASHRAE Transactions*, 116(1).
- Cai, D. W., Adlakha, S., Low, S. H., De Martini, P., & Mani Chandy, K. (2013). Impact of residential PV adoption on Retail Electricity Rates. *Energy Policy*, 62, 830-843.
- California ISO (2013). What the duck curve tells us about managing a green grid. Online source. Accessed on July 10, 2014 from www.caiso.com/documents/flexibleresourceshelprenewables_fastfacts.pdf

Careri, F., Genesi, C., Marannino, P., Montagna, M., Rossi, S., & Siviero, I. (2011). Generation expansion planning in the age of green economy. *Power Systems, IEEE Transactions on*, 26(4), 2214-2223.

Carrasco, J. M., Franquelo, L. G., Bialasiewicz, J. T., Galván, E., Guisado, R. P., Prats, M. A. & Moreno-Alfonso, N. (2006). Power-electronic systems for the grid integration of renewable energy sources: A survey. *Industrial Electronics, IEEE Transactions on*, 53(4), 1002-1016.

Darghouth, N. R., Barbose, G., & Wiser, R. (2011). The impact of rate design and net metering on the bill savings from distributed PV for residential customers in California. *Energy Policy*, 39(9), 5243-5253.

Denholm, P., & Margolis, R. M. (2007). Evaluating the limits of solar photovoltaics (PV) in electric power systems utilizing energy storage and other enabling technologies. *Energy Policy*, 35(9), 4424-4433.

Dexter, A. L., & Haves, P. (1994). Building control systems: evaluation of performance using an emulator. *Building Services Engineering Research and Technology*, 15(3), 131-140.

Duffie, J. A., & Beckman, W. A. (1991). *Solar engineering of thermal processes* (2 ed.). New York: Wiley.

EnergyPlus. (n.d.). *Building Technologies Office: Energy Simulation Software*. Retrieved July 13, 2014, from http://apps1.eere.energy.gov/buildings/energyplus/?utm_source=EnergyPlus&utm_medium=redirect&utm_campaign=EnergyPlus%2Bredirect%2B1.

Erbs, D. G., Klein, S. A., & Duffie, J. A. (1982). Estimation of the diffuse radiation fraction for hourly, daily and monthly-average global radiation. *Solar energy*, 28(4), 293-302.

Erdinc, O., & Uzunoglu, M. (2012). Optimum design of hybrid renewable energy systems: Overview of different approaches. *Renewable and Sustainable Energy Reviews*, 16(3), 1412-1425.

Fernandopulle, N., & Alden, R. T. (2005). Integration of HVDC control dynamics into transient energy functions. *Electrical and Computer Engineering, Canadian Journal of*, 30(1), 17-22.

Fulzele, J. B., & Dutt, S. (2011). Optimum planning of hybrid renewable energy system using HOMER. *International Journal of Electrical and Computer Engineering (IJECE)*, 2(1), 68-74.

Graham, V. A., & Hollands, K. G. T. (1990). A method to generate synthetic hourly solar radiation globally. *Solar Energy*, 44(6), 333-341. GridView. (n.d.). *ABB Grid View*. Retrieved July 13, 2014, from <http://www.abb.us/industries/db0003db004333/c12573e7003305cbc1257013003bddb2.aspx>

Gupta, A., Saini, R. P., & Sharma, M. P. (2011). Modelling of hybrid energy system—Part I: Problem formulation and model development. *Renewable Energy*, 36(2), 459-465.

Hafez, O., & Bhattacharya, K. (2012). Optimal planning and design of a renewable energy based supply system for microgrids. *Renewable Energy*, 45, 7-15.

Hendron, R., & Engebrecht, C. (2010). Building America house simulation protocols.

Hernández-Moro, J., & Martínez-Duart, J. M. (2013). Analytical model for solar PV and CSP electricity costs: present LCOE values and their future evolution. *Renewable and Sustainable Energy Reviews*, 20, 119-132.

HOMER Renewable Energy Software | Distributed Power Design Support. (n.d.). *HOMER Renewable Energy Software | Distributed Power Design Support*. Retrieved July 13, 2014, from <http://www.homerenergy.com/software.html>

Horowitz, S. Program Design Analysis Using BEopt (Building Energy Optimization) Software: Defining a Technology Pathway Leading to New Homes with Zero Peak Cooling Demand.

Hybrid-Renewable Optimization by Genetic Algorithms - English. (n.d.). *Hybrid-Renewable Optimization by Genetic Algorithms - English*. Retrieved July 13, 2014, from <http://hoga-renewable.es.tl/>

International Energy Agency (IEA). Energy technology perspectives 2008: scenarios and strategies to 2050. Paris, France: International Energy Agency, IEA/OECD; 2008. p. 1–650.

Johnson, N., Lilienthal, P., & Schoechle, T. (2011). Modeling distributed premises-based renewables integration using HOMER. Proceedings of 2011 Grid-Interop Conference, Phoenix, AZ.

Katiraei, F., & Aguero, J. R. (2011). Solar PV integration challenges. *Power and Energy Magazine, IEEE*, 9(3), 62-71.

Kempton, W., & Tomić, J. (2005). Vehicle-to-grid power implementation: From stabilizing the grid to supporting large-scale renewable energy. *Journal of Power Sources*, 144(1), 280-294.

Kile, H., & Uhlen, K. (2012). Data reduction via clustering and averaging for contingency and reliability analysis. *International Journal of Electrical Power & Energy Systems*, 43(1), 1435-1442.

Krause, T., Andersson, G., Frohlich, K., & Vaccaro, A. (2011). Multiple-energy carriers: modeling of production, delivery, and consumption. *Proceedings of the IEEE*, 99(1), 15-27.

Laird F.N., 2013. Against transitions? Uncovering conflicts in changing energy systems. *Science as Culture*. 22(2),149-156.

Lambert, T., Gilman, P., & Lilienthal, P. (2006). Micropower system modeling with HOMER. *Integration of alternative sources of energy, I*.

Liu, X., O'Rear, E. G., Tyner, W. E., & Pekny, J. F. (2014). Purchasing vs. leasing: A benefit-cost analysis of residential solar PV panel use in California. *Renewable Energy*, 66, 770-774.

Løken, E. (2007). Use of multicriteria decision analysis methods for energy planning problems. *Renewable and Sustainable Energy Reviews*, 11(7), 1584-1595.

Lovins, A. (2013). *Reinventing fire: Bold business solutions for the new energy era*. Chelsea Green Publishing.

Lund, H. (2005). Large-scale integration of wind power into different energy systems. *Energy*, 30(13), 2402-2412.

Manwell, J. F., & McGowan, J. G. (1993). Lead acid battery storage model for hybrid energy systems. *Solar Energy*, 50(5), 399-405.

MAPS. (n.d.). *Energy Consulting*. Retrieved July 13, 2014, from <http://www.geenergyconsulting.com/practice-area/software-products/maps>

Median and Average Square Feet of Floor Area in New Single-Family Houses Completed by Location. (2010, January 1). . Retrieved July 23, 2014, from <http://www.census.gov/const/C25Ann/sfttotalmedavgsqft.pdf>

Miller, C. A., & Richter, J. (2014). Social Planning for Energy Transitions. *Current Sustainable/Renewable Energy Reports*, 1-8.

Mondol, J. D., Yohanis, Y. G., & Norton, B. (2009). Optimising the economic viability of grid-connected photovoltaic systems. *Applied Energy*, 86(7), 985-999.

Nall, D. H., & Crawley, D. B. (2011). Energy Simulation In the Building Design Process. *ASHRAE Journal*, 53(7).

Negrão, C. O., & Hermes, C. J. (2011). Energy and cost savings in household refrigerating appliances: a simulation-based design approach. *Applied Energy*, 88(9), 3051-3060.

Nemet, A., Klemeš, J. J., Varbanov, P. S., & Kravanja, Z. (2012). Methodology for maximising the use of renewables with variable availability. *Energy*, 44(1), 29-37.

Nguyen, A. T., Reiter, S., & Rigo, P. (2014). A review on simulation-based optimization methods applied to building performance analysis. *Applied Energy*, 113, 1043-1058.

Østergaard, P. A. (2009). Reviewing optimisation criteria for energy systems analyses of renewable energy integration. *Energy*, 34(9), 1236-1245.

Pillai, G. G., Putrus, G. A., Georgitsioti, T., Pearsall, N. M. (2014). Near-term economic benefits from grid-connected residential PV (photovoltaic) systems. *Energy*, 68, 832-843.

PSLF. (n.d.). *Energy Consulting*. Retrieved July 13, 2014, from <http://www.geenergyconsulting.com/practice-area/software-products/pslf>

PSS®NETOMAC. (n.d.). - *Dynamic System Analysis*. Retrieved July 13, 2014, from <http://w3.siemens.com/smartgrid/global/en/products-systems-solutions/software-solutions/planning-data-management-software/planning-simulation/pages/pss-netomac.aspx#>

Purohit, I., & Purohit, P. (2010). Techno-economic evaluation of concentrating solar power generation in India. *Energy Policy*, 38(6), 3015-3029.

Reichelstein, S., & Yorston, M. (2013). The prospects for cost competitive solar PV power. *Energy Policy*, 55, 117-127.

Renewable Energy Optimization Tool. (n.d.). *NREL: Technology Deployment* -. Retrieved July 13, 2014, from http://www.nrel.gov/tech_deployment/tools_reopt.html

RETScreen. (n.d.). *Natural Resources Canada: Empowering Cleaner Energy Decisions*. Retrieved July 13, 2014, from <http://www.retscreen.net/ang/version4.php>

Ruddell, B. L, Salamanca, F., & Mahalov, A. (in review). Reducing a semiarid city's peak electrical demand using distributed cold thermal energy storage. *Applied Energy*, awaiting doi number.

Sadorsky, P. (2012). Modeling renewable energy company risk. *Energy Policy*, 40, 39-48.

Sen, Z. (2008). *Solar energy fundamentals and modeling techniques atmosphere, environment, climate change and renewable energy*. London: Springer.

Sherali, H. D., Soyster, A. L., Murphy, F. H., & Sen, S. (1984). Intertemporal allocation of capital costs in electric utility capacity expansion planning under uncertainty. *Management Science*, 30(1), 1-19.

Siemens PSSE. (n.d.). *Power Transmission System Planning*. Retrieved July 13, 2014, from <http://w3.siemens.com/smartgrid/global/en/products-systems-solutions/software-solutions/planning-data-management-software/planning-simulation/pages/pss-e.aspx#>

Simulation Tool - OpenDSS. (n.d.). *Smart Grid Resource*. Retrieved July 13, 2014, from <http://smartgrid.epri.com/SimulationTool.aspx>

Türkay, B. E., & Telli, A. Y. (2011). Economic analysis of standalone and grid connected hybrid energy systems. *Renewable Energy*, 36(7), 1931-1943.

Ventyx Strategist. (n.d.). *Ventyx: Industrial Software and Insight for Operational Excellence*. Retrieved July 13, 2014, from <http://www.ventyx.com/en/solutions/business-operations/business-products/strategist>

Wang, J., Zhai, Z. J., Jing, Y., Zhang, X., & Zhang, C. (2011). Sensitivity analysis of optimal model on building cooling heating and power system. *Applied Energy*, 88(12), 5143-5152.

Welcome to SAM. (n.d.). *System Advisor Model (SAM) /*. Retrieved July 13, 2014, from <https://sam.nrel.gov/content/welcome-sam>

Wong, P. C., Huang, Z., Chen, Y., Mackey, P., & Jin, S. (2014). Visual Analytics for Power Grid Contingency Analysis. *Computer Graphics and Applications, IEEE*, 34(1), 42-51.

Yun, G. Y., & Steemers, K. (2011). Behavioural, physical and socio-economic factors in household cooling energy consumption. *Applied Energy*, 88(6), 2191-2200.